Short Article

Cell Metabolism

Polyamines and eIF5A Hypusination Modulate Mitochondrial Respiration and Macrophage Activation

Graphical Abstract

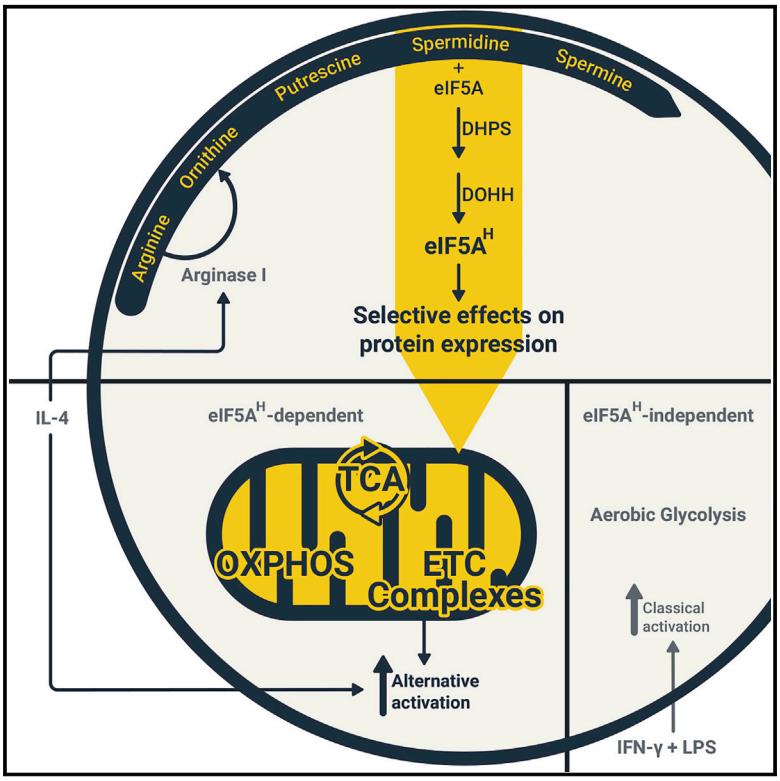

Highlights

- The polyamine synthesis pathway and hypusinated eIF5A modulate mitochondrial OXPHOS
- Hypusinated eIF5A maintains TCA cycle and ETC integrity in macrophages
- Some mitochondrial enzymes depend on eIF5A^{H} for efficient expression
- Inhibition of hypusinated eIF5A blunts macrophage alternative activation

Authors

Daniel J. Puleston, Michael D. Buck, Ramon I. Klein Geltink, ..., Edward J. Pearce, Stefan Balabanov, Erika L. Pearce

Correspondence

pearce@ie-freiburg.mpg.de

In Brief

Puleston et al. show that polyamine biosynthesis modulates mitochondrial metabolism through eIF5A hypusination (eIF5A^{H}). They find that inhibiting the polyamine-eIF5A-hypusine pathway blocks OXPHOS-dependent macrophage alternative activation, while leaving aerobic glycolysis-dependent macrophage classical activation intact. These results might have implications for therapeutically controlling macrophage activation by targeting the polyamine-eIF5A-hypusine axis.

Puleston et al., 2019, Cell Metabolism *30*, 352–363
August 6, 2019
https://doi.org/10.1016/j.cmet.2019.05.003

CellPress

CellPress

Cell Metabolism
Short Article

Polyamines and eIF5A Hypusination Modulate Mitochondrial Respiration and Macrophage Activation

Daniel J. Puleston,[1,2] Michael D. Buck,[1,9] Ramon I. Klein Geltink,[1,9] Ryan L. Kyle,[1] George Caputa,[1] David O'Sullivan,[1] Alanna M. Cameron,[1] Angela Castoldi,[1] Yaarub Musa,[1] Agnieszka M. Kabat,[1] Ying Zhang,[3] Lea J. Flachsmann,[1] Cameron S. Field,[1] Annette E. Patterson,[1] Stefanie Scherer,[4] Francesca Alfei,[4] Francesc Baixauli,[1] S. Kyle Austin,[1] Beth Kelly,[1] Mai Matsushita,[1] Jonathan D. Curtis,[1] Katarzyna M. Grzes,[1] Matteo Villa,[1] Mauro Corrado,[1] David E. Sanin,[1] Jing Qiu,[1] Nora Pällman,[5] Katelyn Paz,[6] Maria Elena Maccari,[7] Bruce R. Blazar,[6] Gerhard Mittler,[1] Joerg M. Buescher,[1] Dietmar Zehn,[4] Sabine Rospert,[3] Edward J. Pearce,[1,8] Stefan Balabanov,[5] and Erika L. Pearce[1,10,*]

[1]Max Planck Institute of Immunobiology and Epigenetics, Freiburg 79108, Germany
[2]The Kennedy Institute of Rheumatology, University of Oxford, Oxford OX3 7FY, UK
[3]Institute of Biochemistry and Molecular Biology, ZBMZ, Faculty of Medicine, and BIOSS Centre for Biological Signaling Studies, University of Freiburg, Freiburg 79104, Germany
[4]Department of Animal Physiology and Immunology, Technical University of Munich, Freising, Germany
[5]Division of Haematology, University Hospital Zurich and University of Zurich, Zurich 8091, Switzerland
[6]Department of Pediatrics, Division of Blood and Marrow Transplantation, University of Minnesota, Minneapolis, MN, USA
[7]Institute for Immunodeficiency, Center for Chronic Immunodeficiency, Center for Pediatrics, and Faculty of Medicine, Medical Center - University of Freiburg, Freiburg 79106, Germany
[8]Faculty of Biology, University of Freiburg, Freiburg 79104, Germany
[9]These authors contributed equally
[10]Lead Contact
*Correspondence: pearce@ie-freiburg.mpg.de
https://doi.org/10.1016/j.cmet.2019.05.003

SUMMARY

How cells adapt metabolism to meet demands is an active area of interest across biology. Among a broad range of functions, the polyamine spermidine is needed to hypusinate the translation factor eukaryotic initiation factor 5A (eIF5A). We show here that hypusinated eIF5A (eIF5A^{H}) promotes the efficient expression of a subset of mitochondrial proteins involved in the TCA cycle and oxidative phosphorylation (OXPHOS). Several of these proteins have mitochondrial targeting sequences (MTSs) that in part confer an increased dependency on eIF5AH. In macrophages, metabolic switching between OXPHOS and glycolysis supports divergent functional fates stimulated by activation signals. In these cells, hypusination of eIF5A appears to be dynamically regulated after activation. Using *in vivo* and *in vitro* models, we show that acute inhibition of this pathway blunts OXPHOS-dependent alternative activation, while leaving aerobic glycolysis-dependent classical activation intact. These results might have implications for therapeutically controlling macrophage activation by targeting the polyamine-eIF5A-hypusine axis.

INTRODUCTION

Aberrant metabolic rewiring can have pathological consequences. This is evident in cells of the immune system, where metabolic pathways and their metabolites not only provide energy and substrates for growth and survival, but also instruct differentiation, gene expression, and effector functions important

Context and Significance

Macrophages play key physiological roles, including combating infections and cancer. The underlying metabolism of macrophages is linked to their function and modulation of metabolic pathways in immune cells for therapeutic purposes is an active area of investigation. Researchers at the Max Planck Institute in Freiburg, Germany, discovered that a fundamental metabolic pathway (polyamine biosynthesis), which had previously been linked to essential cellular processes, such as DNA repair, is intricately involved in cellular respiration and macrophage function by regulating mitochondrial proteins. Polyamine biosynthesis results in a specific chemical modification (hypusination) of the enzyme eIF5A that regulates a subset of mitochondrial proteins involved in core respiration, thus affecting alternative macrophage activation, a cell type that strongly engages their mitochondria. These results put the polyamine pathway and hypusination on the therapeutic map for immune cells.

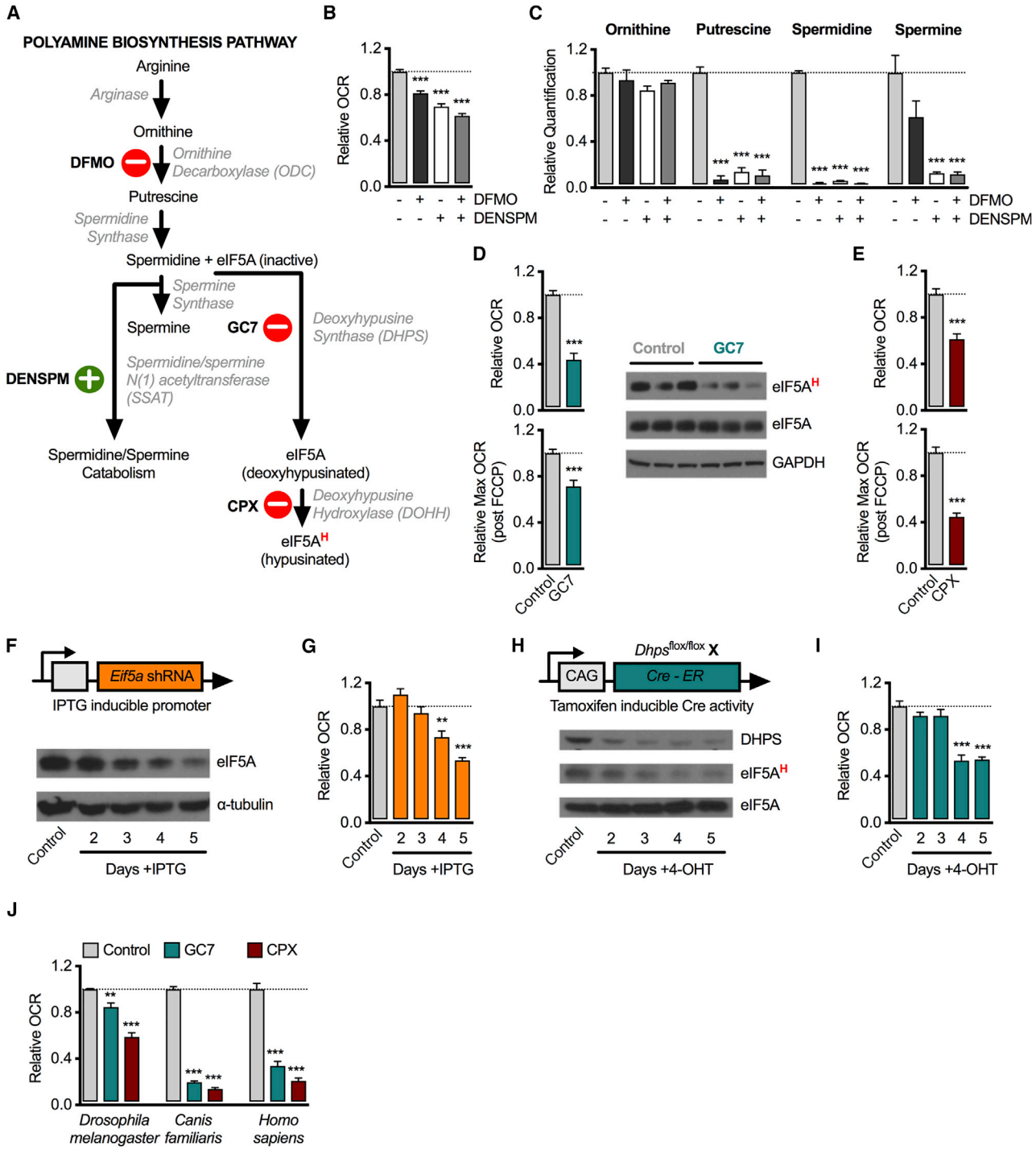

Figure 1. The Polyamine Synthesis Pathway and Hypusinated eIF5A Modulates OXPHOS

(A) The polyamine pathway comprises the cationic metabolites putrescine, spermidine, and spermine, which are synthesized downstream of the amino acid ornithine. Spermidine acts as a substrate for the hypusination of eIF5A, catalyzed by DHPS and DOHH. DFMO inhibits ODC, whereas DENSPM induces polyamine catabolism. Both GC7 and CPX inhibit hypusination.

(B) Relative OCR of MEFs (NIH-3T3) incubated for 48 h with 2.5 mM DFMO ± 50 μM DENSPM assessed by Seahorse Extracellular Flux Analyzer (relative OCR = OCR of treated cells normalized to OCR of untreated control cells).

(C) Intracellular ornithine, putrescine, spermidine, and spermine levels detected by LC-MS of MEFs treated as in (B).

(D) Relative OCR, maximum OCR, and western blot analysis of eIF5A^{H} levels in MEFs treated with 10 μM GC7 for 24 h (relative OCR = basal OCR of treated cells normalized to basal OCR of untreated control cells).

(legend continued on next page)

for host immunity and tissue homeostasis (Buck et al., 2017). Understanding how immune cells control metabolic pathways, engaging one or dampening another, may provide valuable insight into controlling cellular functions by redirecting metabolism.

Polyamines have roles in cellular proliferation, autophagy, binding DNA, and modulating ion channels (Miller-Fleming et al., 2015; Pegg, 2016). In eukaryotes, the polyamine spermidine also serves as a substrate for the hypusination of a conserved lysine residue in eukaryotic initiation factor 5A (eIF5A) (Park et al., 1981) by the action of two enzymes, deoxyhypusine synthase (DHPS) and deoxyhypusine hydroxylase (DOHH) (Abbruzzese et al., 1986; Wolff et al., 1995). There are two isoforms of eIF5A, eIF5A1 (we refer to this isoform as eIF5A in this study), which is expressed ubiquitously, and eIF5A2, which is only expressed in the testes and brain (Jenkins et al., 2001). Although originally thought to initiate translation, eIF5A^{H} actually promotes general translation elongation and termination (Saini et al., 2009) (Schuller et al., 2017). It has also been linked to the efficient translation of select mRNA subsets (Kang and Hershey, 1994), such as those containing consecutive proline codons (Gutierrez et al., 2013), or other sequence-specific properties (Pelechano and Alepuz, 2017). Although polyamine levels are elevated in most cancers, and eIF5A is recognized as a critical regulator of cell growth and tumor development (Nakanishi and Cleveland, 2016), precisely how these pathways coordinate to support cell metabolism in healthy cells is unclear.

RESULTS

Polyamine Synthesis and Hypusinated eIF5A Modulate OXPHOS

To investigate how polyamine biosynthesis (Figure 1A) contributes to metabolism we exposed murine embryonic fibroblasts (MEFs) to 2-difluoromethylornithine (DFMO), an inhibitor of ornithine decarboxylase (ODC) (Poulin et al., 1992), the enzyme that initiates polyamine synthesis, and diethylnorspermine (DENSPM), which induces the spermidine catabolizing enzyme SSAT and spermidine oxidase (Stanić et al., 2009). Blocking polyamine biosynthesis, or inducing spermidine catabolism, reduced oxygen consumption rates (OCRs) (an indicator of oxidative phosphorylation [OXPHOS]), while also reducing extracellular acidification rates (ECARs) (an indicator of aerobic glycolysis), although to a lesser extent (Figures 1B, S1A, and S1B). We confirmed a decrease in putrescine, spermidine, and spermine levels in treated cells, whereas the upstream metabolite ornithine was unchanged (Figure 1C). An important cellular function of spermidine is to provide a substrate for DHPS, the rate-limiting enzyme during eIF5A^{H} formation (Park et al., 1981) (Figure 1A). Cells exposed to the DHPS inhibitor GC7 (Melis et al., 2017), or ciclopirox (CPX), a DOHH inhibitor (Hoque et al., 2009), also dampened OXPHOS (Figures 1D and 1E). Immunoblot with an eIF5A^{H}-specific antibody (Nishiki et al., 2013) confirmed that eIF5A^{H} was decreased after GC7 treatment.

Although pharmacological inhibitors often have off-target effects, which can confound results, they also can permit the acute inhibition of a particular target. As long as results are interpreted cautiously, this approach can be helpful when studying a pathway as central as respiration. Genetic evidence can support inhibitor studies, but also must be interpreted carefully, as genetic models often result in a more chronic deletion, depending on the techniques used to delete a specific gene. With these caveats in mind, we examined the loss of respiration genetically by acutely knocking down components of this pathway. We transduced isopropyl β-D-1-thiogalactopyranoside (IPTG)-inducible *Eif5a*-small hairpin RNA (shRNA) into MEFs (Figures 1F and S1C) and observed a direct correlation between eIF5A expression and respiration (Figure 1G). Cells with tamoxifen-induced deletion of *Dhps* (Figure 1H) displayed a similar loss of OCR (Figure 1I), while these treatments had varying effects on ECARs (Figures S1D–S1H). Cell viability was unaffected in drug-treated MEFs (data not shown) and in those expressing *Eif5a*-shRNA for 5 days (Figure S1I). Collectively, our results show that dampening any one of several components of the polyamine-eIF5A^{H} pathway, either by acute pharmacological or genetic inhibition, limits OXPHOS, a process conserved across cell types and species (Figures 1J and S1J).

Hypusinated eIF5A Maintains Tricarboxylic Acid Cycle and *ETC* Integrity in Macrophages

To assess the extent of this respiration defect, we exposed MEFs to 2-deoxyglucose, which enforces OXPHOS by limiting glycolysis. MEFs expressing *Eif5a*-shRNA, or depleted for *Dhps*, did not compensate by enhancing OCRs compared with controls (Figures S1K–S1N), revealing that, when forced, cells with insufficient levels of eIF5A or eIF5A^{H} are unable to promote mitochondrial respiration in this setting. To further probe respiratory function controlled by eIF5A, we generated mouse bone-marrow-derived macrophages (BMMφ) and then activated them with interleukin-4 (IL-4) (M(IL-4)). IL-4-driven activation of these cells depends on mitochondrial respiration (Vats et al., 2006), while lipopolysaccharide (LPS)/interferon γ (IFN-γ)-driven activation depends on aerobic glycolysis (Tannahill et al., 2013). Since M(IL-4) and LPS/IFN-γ-activated macrophages (M(LPS/IFN-γ)) do not proliferate to an appreciable extent *in vitro* (Arpa et al., 2009; Liu et al., 2016), we could assess the role of polyamine biosynthesis on respiration dissociated from its regulation

(E) Relative OCR (relative OCR = basal OCR of treated cells normalized to basal OCR of untreated control cells) and maximum OCR (OCR post-FCCP injection) in MEFs treated with 20 μM CPX for 24 h (OCR is normalized to the baseline OCR of untreated cells).

(F and G) Immunoblot analysis of eIF5A (F) and relative OCR of MEFs (NIH-3T3) expressing isopropyl β-D-1-thiogalactopyranoside (IPTG)-inducible *Eif5a*-shRNA (G). Cells were treated with 100 μM IPTG for the indicated length of time. OCR is normalized to the baseline OCR of non-IPTG-treated control cells.

(H and I) Western blot of DHPS, total eIF5A, and eIF5A-hypusine levels (H) and relative OCR in *Dhps*$^{flox/flox}$ MEFs expressing a 4-OHT-inducible Cre (Cre-ER) (controls are 4-OHT-treated *Dhps*$^{flox/flox}$ Cre-ER^{-} cells) (I). OCR is normalized to the baseline OCR of control cells. Cells were treated with 10 μM 4-OHT for the indicated length of time.

(J) S2 (*D. melanogaster*), Madin-Darby Canine Kidney (MDCK) (*C. familiaris*), and MCF-7 (*H. sapiens*) cells treated with 10 μM GC7 and 20 μM CPX for 24 h. All data are means ± SEM ($p^{**} < 0.005$, $p^{***} < 0.0005$, compared with control or untreated). (B)–(E) and (J) Representative of two experiments and (F)–(I) representative of three experiments.

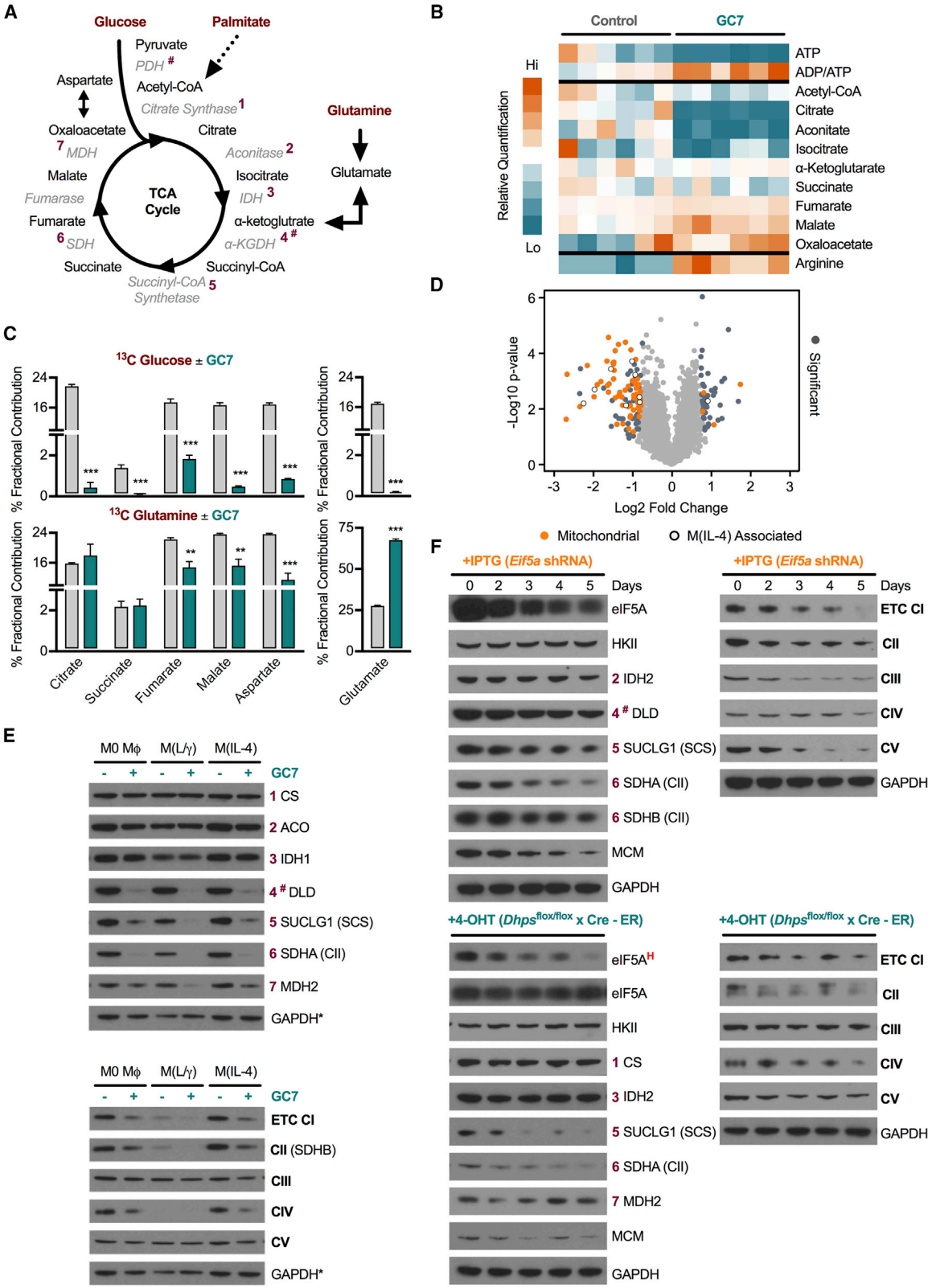

Figure 2. Hypusinated eIF5A Maintains TCA Cycle and ETC Integrity in Macrophages

(A) TCA cycle schematic highlighting points of entry for glucose, palmitate, and glutamine.

(B) LC-MS quantification of indicated metabolites in M(IL-4) exposed to 10 μM GC7 for 24 h, relative to control cells.

(legend continued on next page)

of proliferation (Figure S1O) (Thomas and Thomas, 2001). Similar to the data from MEFs, ablating eIF5A^{H}, either genetically or pharmacologically (Figures S1P and S1Q), blocked respiration in M(IL-4) (Figures S1R–S1T), while having varying effects on ECARs (Figures S1U–S1W).

To probe how eIF5A^{H} affects respiration, we analyzed *Eif5a*-shRNA-expressing MEFs and GC7-treated M(IL-4) by liquid chromatography-mass spectrometry (LC-MS) and found decreased metabolites associated with the first half of the tricarboxylic acid (TCA) cycle (Figures 2A, 2B, and S2A), as well as additional alterations in other metabolic pathways (Figures S2B and S2C). Next, we cultured M(IL-4) with ^{13}C-labeled glucose, glutamine, or palmitate and traced carbon from these substrates into metabolites. GC7-treated M(IL-4) incorporated significantly less carbon from ^{13}C-glucose into TCA cycle metabolites compared with control cells (Figure 2C), indicating that DHPS function, and thus eIF5A^{H}, is needed for TCA cycle engagement. Incorporation of ^{13}C-glutamine and palmitate carbons into TCA cycle metabolites was also decreased in GC7-treated cells (Figures 2C and S2D).

eIF5A^{H} Ablation Dampens the Expression of Some Mitochondrial Proteins

To ascertain why TCA cycle flux was inhibited, we performed a proteomics analysis of GC7-treated M(IL-4). Of 153 significantly altered proteins, 63 were mitochondrial, including TCA cycle enzymes and ETC proteins (Figure 2D and Table S1). The one factor that we had uncovered thus far that unified our results was that, on acute pharmacologic or genetic inhibition of any one of several components of the polyamine-eIF5A^{H} pathway, we observed decreased OXPHOS, which was consistent with dysregulated mitochondrial metabolism. We investigated if this perturbation in the mitochondrial proteome highlighted by our proteomic analysis was the cause of defective mitochondrial respiration in the absence of eIF5A^{H}.

To validate our proteomics data, we assessed the expression of several mitochondrial enzymes, for which there were high quality commercial antibodies available, in GC7-treated BMMφ (Figure 2E), *Eif5a*-shRNA-expressing MEFs, or *Dhps*$^{flox/flox}$ MEFs expressing Cre-ER (Figure 2F) by western blot. In cells with reduced eIF5A or eIF5A^{H} we found decreased expression of several TCA proteins, including succinyl-CoA synthetase (SUCLG1) and succinate dehydrogenase (SDH), supporting the observed break in the TCA cycle (Figures 2B, 2C, and S2D). Other proteins such as citrate synthase and isocitrate dehydrogenase (IDH) were less affected (Figures 2E, 2F, and S2E). Enzymes that feed substrates into the TCA cycle, such as methylmalonyl-CoA mutase (MCM) and pyruvate dehydrogenase, were also diminished after *Eif5a* or *Dhps* deletion, or treatment with GC7 (Figures 2F and S2F). However, the expression of many enzymes in glycolysis, fatty acid synthesis, and the aspartate-argininosuccinate shunt remained stable (Figures S2G and S2H), which suggested that there was not a defect in general translation. Exposing M(IL-4) or lymphoma cells to polyamine synthesis inhibitors or CPX also resulted in deficiencies in specific TCA cycle enzymes (Figures S2I–S2K).

Since SDH has a dual role and also participates in the ETC as complex II, we assayed ETC complexes and found that GC7-treated M0 and M(IL-4) and MEFs deleted for *Eif5a* and *Dhps* (Figures 2E and 2F) had dampened expression of several ETC complex proteins. M(LPS/IFN-γ) had decreased expression of these ETC proteins regardless of GC7 treatment (Figure 2E). Consistent with decreased TCA cycle metabolites in GC7-treated cells (Figure 2B), we observed a partial rescue of respiration on exposure to succinate (Figure S2L). Together, these data suggest that the polyamine-eIF5A^{H} axis supports the expression of a subset of mitochondrial proteins in core respiration, providing a possible explanation as to why cells with decreased eIF5A^{H} have reduced TCA cycle flux and OCRs.

We next assessed how eIF5A^{H} might specifically regulate mitochondrial protein expression, and thereby OXHPOS. Although many mitochondrial proteins were strikingly decreased 24 h following GC7 treatment (Figure 2E), transcription of the genes encoding these proteins was not diminished 24 h following GC7 treatment (Figure 3A), indicating that the TCA cycle defects conferred by reduced eIF5A^{H} were not necessarily a direct reflection of transcriptional changes in these genes. Polyamines and eIF5A are also known to modulate autophagy (Eisenberg et al., 2009; Lubas et al., 2018), an important process controlling mitochondrial quality (Pickles et al., 2018). However, M(IL-4) macrophages treated with the autophagy inhibitor bafilomycin A1 displayed normal expression of numerous mitochondrial proteins (Figure S3A), suggesting to us that, at least in the context we were investigating, autophagy was not playing a direct role.

Certain MTSs Have an Increased Dependency on eIF5A^{H}

To explore how eIF5A might exert control over the translation of specific mRNAs, we performed polysome analysis of control and *Eif5a*-shRNA-expressing MEFs. Polysomes are thought to be a major site of active translation (Van Der Kelen et al., 2009). We speculated that there might be a selective loss of gene transcripts from polysomes that corresponded to the proteins identified in our proteomics data as displaying a greater dependency on eIF5A^{H} (Table S1). Polysome profile analysis revealed reduced polysomes in eIF5A-depleted cells (Figure 3B), in line with previously published data and known translation defects on eIF5A ablation (Henderson and Hershey, 2011). Consistent with reduced polysomes, we observed that the transcripts for eIF5A hyperdependent *Sdha* and *Mcm* moved out of the polysome fraction after eIF5A deletion, but the same was true for *Idh2* and *Gapdh* transcripts, two proteins that did not show

(C) D-^{13}C-Glucose and ^{13}C-glutamine gas chromatography-mass spectrometry trace analysis of M(IL-4) treated with 10 μM GC7 for 24 h.
(D) Proteomic analysis of M(IL-4) treated with 10 μM GC7 for 24 h.
(E and F) Immunoblot assessment of selected TCA cycle enzymes, as depicted in (A), and ETC-associated proteins in (E) M0, M(LPS/IFN-γ) = M(L/γ), and M(IL-4) treated with 10 μM GC7 for 22 h, and in (F) MEFs (NIH-3T3) transduced with *Eif5a*-shRNA for the indicated amount of days or *Dhps*$^{flox/flox}$ Cre-ER MEFs treated with 4-OHT for the stated length of time. All data are means ± SEM ($p^{**} < 0.005$, $p^{***} < 0.0005$). (B and C) Representative of two experiments, (D) of one experiment (n = 3/group), and (E and F) of three experiments. *Duplicate loading control. Due to overlapping sizes, loading controls were analyzed on separate gels. Same amount of protein was run for analyses (E).

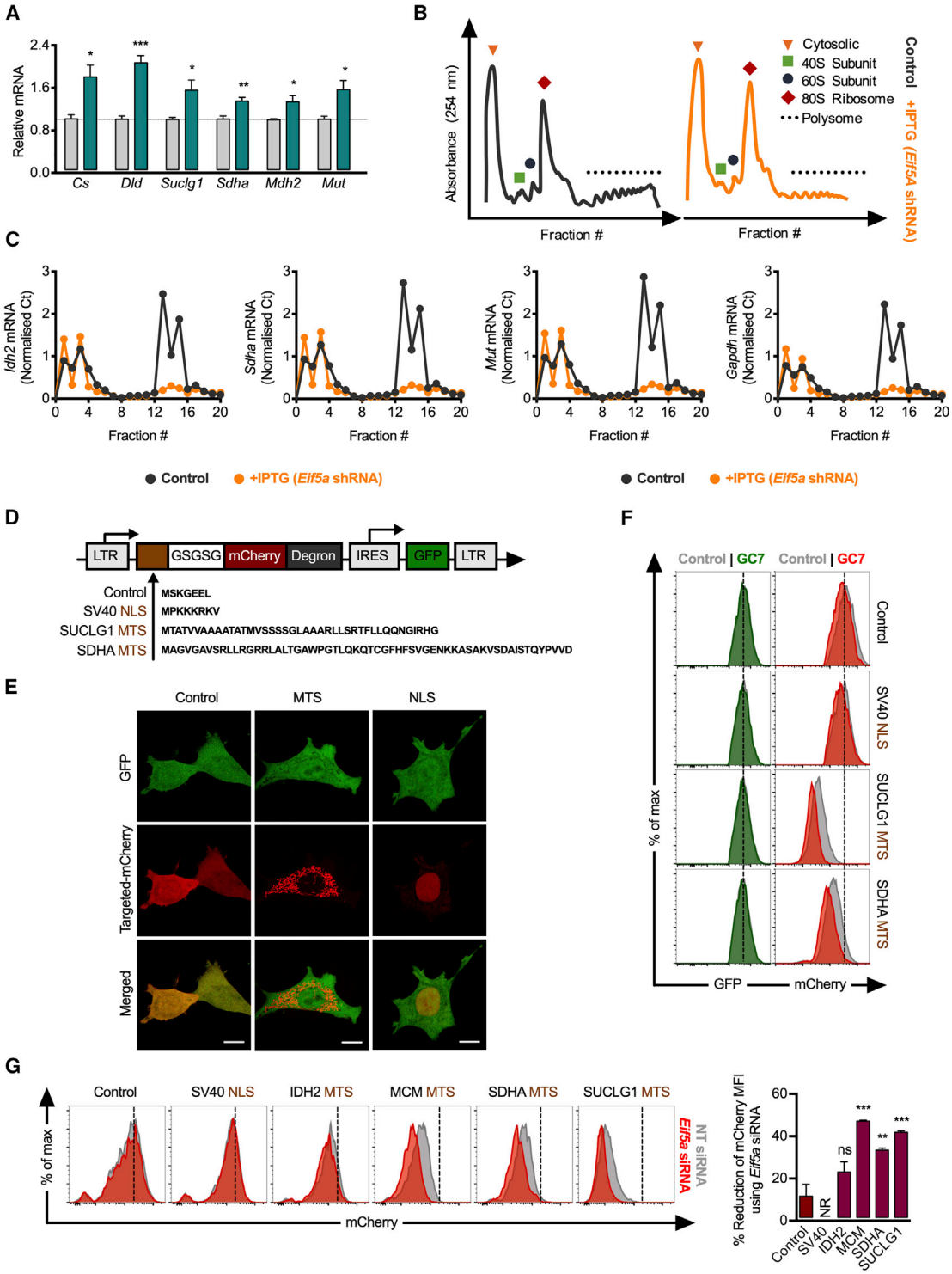

Figure 3. The MTS of Several Mitochondrial Enzymes Exhibit an Increased Dependency on eIF5A^{H} for Efficient Translation

(A) Relative mRNA expression of indicated genes in M(IL-4) treated with 10 μM GC7 for 24 h.

(B) Polysome profiles of MEFs (NIH-3T3) expressing *Eif5a*-shRNA for 5 days versus control MEFs. The y axis indicates absorption at 254 nm, and the x axis represents fractions separated over a 15%–55% sucrose gradient.

(C) RT-PCR analysis of indicated mRNAs in ribosome fractions generated from control and *Eif5a*-shRNA-expressing MEFs (NIH-3T3).

(D) Target sequences were cloned into the N terminus of mCherry fused to a degron (to limit its half-life and circumvent differential MTS mCherry half-life between constructs) separated by a GSGSG flexible linker to allow correct and independent folding of the introduced sequences and mCherry. These were subcloned into the MIGR1 vector and transduced into MEFs (SUCLG1 is a subunit of succinyl-CoA synthetase).

(legend continued on next page)

increased dependency on eIF5A^H in our experiments (Figure 3C). Although these observations were consistent with a role of eIF5A in general translation (Pelechano and Alepuz, 2017; Schuller et al., 2017), these data did not provide us with further insight into a mechanism of how specific mitochondrial proteins could have an increased dependency on eIF5A for efficient translation, and suggested that differences might occur during translation elongation in monosomes (Heyer and Moore, 2016).

To approach this question in a targeted fashion, we reasoned that ~40% of the proteins we found to be sensitive to eIF5A inhibition were mitochondrial proteins, and therefore contained a MTSs (Table S1). MTSs contain motifs, such as stretches of repetitive amino acids or a high frequency of charged residues, which can lead to ribosome stalling and slower translation (Charneski and Hurst, 2013; Sabi and Tuller, 2015). To test whether MTSs of specific mitochondrial proteins could increase dependency on eIF5A^H for efficient expression we cloned the MTSs of several proteins (SUCLG1, SDHA, and MCM) identified by our proteomic and immunoblot analyses (Table S1; Figures 2E and 2F) to be eIF5A^H-hyperdependent and fused them to the N terminus of mCherry in MIGR1. We chose these proteins based on them having known MTS sequences that we were able to validate. In the context of these constructs, mCherry expression would rely on the translation of the preceding sequence (Figures 3D and S3B). As controls, in place of the MTSs, we positioned a SV40 nuclear localization sequence (NLS) and a control amino acid sequence made up of the first seven residues of GFP at the N terminus of mCherry (herein referred to as "control") (Figure 3D). For comparison, we examined the MTSs of IDH2 (Figure S3B), a protein suggested by our immunoblot analyses to have reduced dependency on eIF5A^H (Figures 2F and S2E). We imaged cells to confirm that our MTS mCherry constructs localized to mitochondria, and SV40 NLS mCherry to the nucleus (Figures 3E and S3C). Next, we transduced these constructs into MEFs and assessed mCherry expression by flow cytometry in the presence of *Eif5a*-small interfering RNA (siRNA), *Dhps*-siRNA, to acutely genetically target this pathway, or GC7, for acute pharmacological inhibition. Importantly, internal ribosome entry site (IRES)-driven GFP expression was equivalent in cells transduced with all constructs, and unaffected by genetic or pharmacological deletion of *Dhps* or *Eif5a* (Figure 3F).

Compared with control cells, or cells exposed to a nontargeted siRNA, mCherry expression dependent on SUCLG1, SDHA, or MCM MTSs was decreased compared with control or NLS mCherry (Figures 3F, 3G, and S3D). These data suggest that, regardless of a reduction in eIF5A or eIF5A^H (Figure S3E), the MTSs of these proteins have reduced translation, consistent with our hypothesis that these eIF5A^H-dependent mitochondrial proteins have MTSs that could lead to slower/less efficient translation. In contrast, IDH2 MTS mCherry was more highly expressed, in line with IDH2 protein being unaffected by the loss of eIF5A^H (Figure S3D). When we exposed transduced cells to *Eif5a*-siRNA, *Dhps*-siRNA, or GC7 the expression of SUCLG1, SDHA, and MCM MTS mCherry was further abrogated relative to untreated cells or cells exposed to a nontargeted siRNA (Figures 3F, 3G, and S3F). This effect was much less apparent on IDH2 MTSs, SV40 NLS, and control mCherry expression.

To confirm that the MTSs of select mitochondrial proteins contain amino acid sequences that confer eIF5A hyperdependency, we swapped the C terminus half of the IDH2 MTSs for the C terminus half of SUCLG1 MTSs and fused that novel sequence to the N terminus of mCherry. Whereas normal IDH2 MTSs translation exhibited little sensitivity to GC7, the domain swap of C terminus SUCLG1 MTSs resulted in significantly decreased translation in response to GC7 (Figure S3G). Normal SUCLG1 MTS translation exhibited high sensitivity to eIF5A^H inhibition; however, when we fused the N terminus half of SUCLG1 MTSs to the C terminus half of IDH2 MTSs at the beginning of mCherry, we observed no decrease in translation of this product in response to GC7 (Figure S3G). These data suggest that sequences in SUCLG1 MTSs require eIF5A^H for optimal translation, while the IDH2 MTS sequence has a comparatively reduced requirement for eIF5A^H, explaining the loss of SUCLG1 protein, but normal IDH2 levels during eIF5A^H ablation. These observations support our conclusion that, for this set of proteins examined, the MTS sequences lead to slower translation and therefore show increased dependency on eIF5A^H, a protein known to facilitate efficient translation of transcripts with specific sequence properties (Pelechano and Alepuz, 2017; Schuller et al., 2017).

A Role for eIF5A^H in Regulating Differential Macrophage Activation

We next wanted to delineate the housekeeping function of eIF5A^H from its apparent function in specifically modulating mitochondrial respiration. Given that immune cell activation causes changes in the level of engagement of respiration, we investigated whether hypusine formation could be dynamically regulated in response to immune stimuli. We analyzed eIF5A and eIF5A^H expression in M(LPS/IFN-γ) and M(IL-4) at various times after activation. With the exception of 4 h after stimulation, eIF5A^H was not increased in BMMφ following exposure to LPS/IFN-γ, while eIF5A^H was induced after activation with IL-4 (Figure 4A), demonstrating that eIF5A^H levels are modulated in response to these different immune stimuli. The increased eIF5A^H apparent in M(IL-4) after activation correlated with an enrichment in the expression of hypusinating enzymes in these cells compared with M(LPS/IFN-γ) (Figure S4A). We also observed an increase in the flux of arginine into putrescine in M(IL-4) compared with M(LPS/IFN-γ) (Figure 4B), suggesting that dynamic regulation of substrates

(E) Representative confocal images of cloned constructs SV40 NLS-, IDH2 MTS-, and control mCherry. Scale bar, 10 μm.
(F) Representative histograms of indicated constructs in MEFs (NIH-3T3) ± 10 μM GC7 for 24 h.
(G) Indicated constructs were transfected with *Eif5a* siRNA plus a nontargeting AF647-labeled siRNA as a control for transfection into MEFs (NIH-3T3). Control cells only received nontargeting siRNA. mCherry mean fluorescence intensity (MFI) was assessed 48 h after transfection by flow cytometry. Shown are representative histograms. Histograms are gated on GFP$^+$ AF647$^+$ cells. Bar graphs depict percent reduction of mCherry MFI between *Eif5a* siRNA and nontargeting siRNA: NS, nonsignificant; NR, no reduction in mCherry (n = 3/group). All data are means ± SEM ($p^* < 0.05$, $p^{**} < 0.005$, $p^{***} < 0.0005$). (A) Representative of two to three experiments (n = 3 per group), (B and C) of one experiment, (E) of two experiments, and (F and G) of three to four experiments.

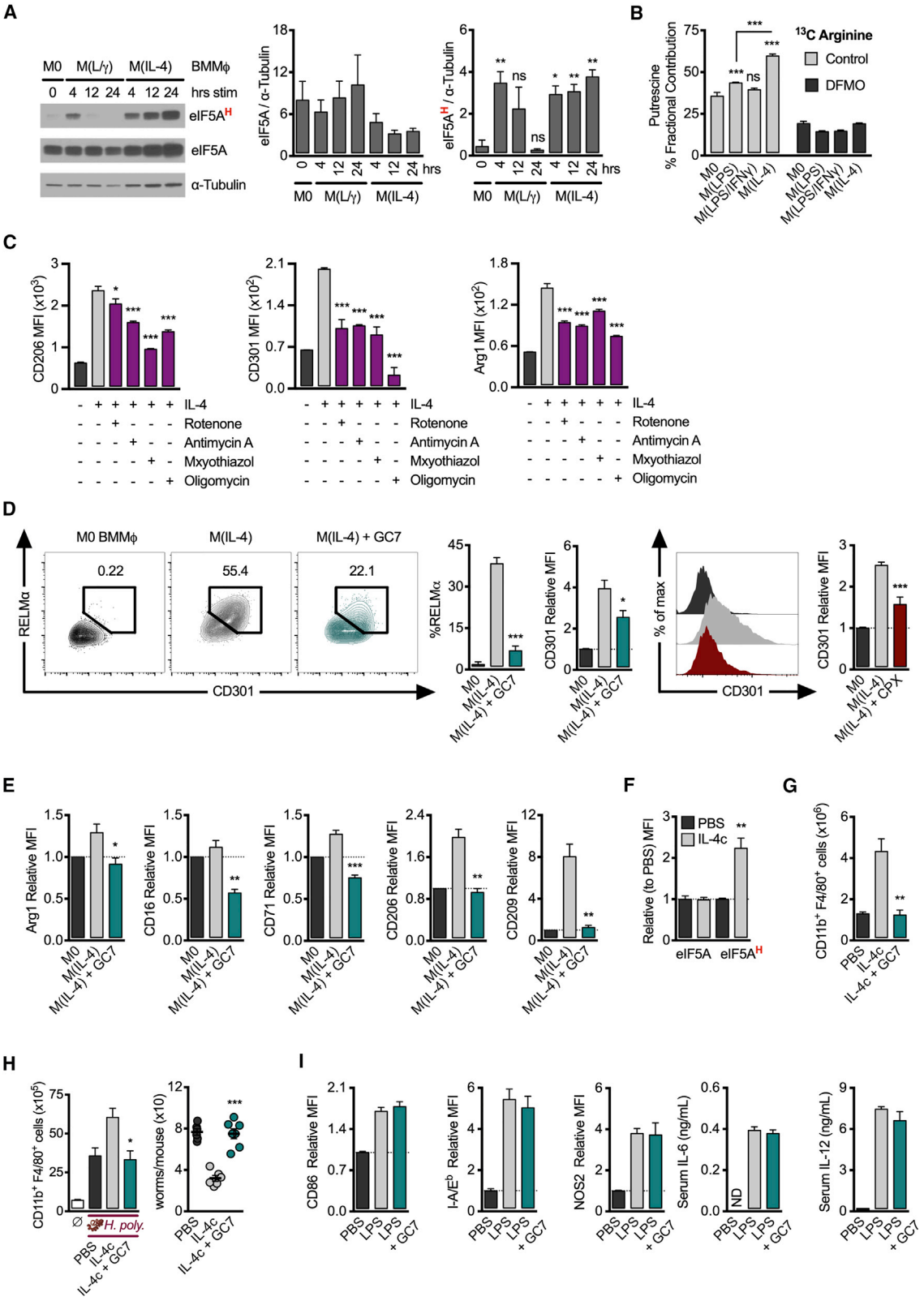

Figure 4. A Role for eIF5A^H in Differential Macrophage Activation

(A) Immunoblot analysis and densitometry of eIF5A and eIF5A^H levels in BMMφ exposed to LPS plus IFN-γ or IL-4 for the indicated length of time. Representative of three individual mice.

(legend continued on next page)

from polyamine biosynthesis could lead to alterations in eIF5A^{H} levels in immune cells.

Previously, OXPHOS has been implicated in M(IL-4) activation (Huang et al., 2014; Van den Bossche et al., 2016; Vats et al., 2006). To test this directly we activated BMMφ with IL-4 in the presence or absence of mitochondrial inhibitors. We observed significantly impaired expression of CD206, CD301, and Arg1 during complex I inhibition (with rotenone), complex III inhibition (with antimycin A and myxothiazol), and complex V inhibition (with oligomycin), supporting that mitochondrial respiration is important for macrophage alternative activation (Figures 4C and S4B). We next assessed markers of alternative activation in M(IL-4) on acute eIF5A^{H} inhibition. Reducing eIF5A^{H} blunted RELMα expression (Figures 4D and S4C), while GC7 and CPX treatment, or genetic ablation of *Eif5a*, *Dhps*, or *Dohh*, blunted Arg1, CD301, and CD206 to varying degrees (Figures 4D and S4D–S4G), indicating reduced alternative activation, despite intact IL-4 signaling through STAT6 (Figure S4H). Proteomics data of GC7-treated M(IL-4) confirmed the decline of many proteins associated with alternative activation, including CD301 (Figure 2D; Table S1). Human monocyte-derived macrophages exposed to IL-4 also exhibited increased eIF5A^{H} (Figure S4I) and GC7 treatment potently reduced expression of alternative activation markers in these cells (Figures 4E and S4J), suggesting that eIF5A^{H} is also required for human M(IL-4) activation. To test if IL-4 could induce eIF5A^{H} *in vivo*, we administered IL-4 as a complex (IL-4c) into the peritoneal cavity of mice and assessed eIF5A and eIF5A^{H} expression. While total eIF5A levels remained stable following exposure to IL-4c, eIF5A^{H} was significantly increased, again illustrating that hypusination is a dynamically regulated process in macrophages (Figure 4F). Furthermore, the *in situ* peritoneal accumulation of macrophages in response to IL-4c, a hallmark of alternative activation *in vivo* (Jenkins et al., 2011), was diminished in the presence of GC7 (Figure 4G). These data support the idea that eIF5A^{H} has a prominent role in macrophages that rely on OXPHOS.

To further test the function of eIF5A^{H} in alternative macrophage activation and protective immunity *in vivo*, we infected mice with the intestinal helminth parasite *Heligmosomoides polygyrus*. Mice were pre-treated with IL-4c on days −4, −2, and 0 before infection to drive the expansion of alternatively activated macrophages. Some mice were injected daily with GC7 between days −4 and 0. This experimental design allowed us to more specifically target macrophages without directly affecting the ensuing T cell response. On day 15 after infection we found significantly increased numbers of macrophages in the peritoneal cavity alongside a reduced number of worms in the intestines, and eggs in the feces when mice were pre-treated with IL-4 (Figures 4H and S4K). This effect was lost in mice pre-treated with GC7, indicating reduced alternative macrophage polarization (Figures 4H and S4K). We saw no reduction of the T_H2 response after GC7 (data not shown).

Consistent with the idea that eIF5A^{H} activity is most critical in cells that depend on increased respiration, markers of classical macrophage activation, such as nitric oxide synthase 2 (NOS2), major histocompatibility complex class II (MHCII), and CD86 were unchanged in M(LPS/IFN-γ), cells that rely on aerobic glycolysis, following genetic or pharmacological targeting of components of the eIF5A^{H} pathway (Figures S4L–S4N). To substantiate these observations *in vivo*, we injected LPS into the peritoneal cavity of mice to elicit classical macrophage activation. Macrophages from mice coinjected with GC7 maintained CD86, MHCII, NOS2, and serum IL-6 and IL-12 levels similar to those in controls treated with LPS alone (Figure 4I). Together these data suggest that classical macrophage activation remained unchanged after GC7 treatment.

DISCUSSION

Many inhibitors have off-target effects; however, they remain valuable tools. Genetic models can also come with caveats, as they usually present a longer-term, more chronic deletion that can confound more proximal effects that occur when a gene is initially deleted. We have taken a broad approach in this study using many compounds and acute genetic deletion models to probe the polyamine-eIF5A^{H} axis. The blend of these approaches has led us to conclude that the polyamine-eIF5A^{H} axis plays a role in regulating mitochondrial respiration, at least in part, by influencing the expression of distinct subset of mitochondrial enzymes. Our findings are supported by a report that genetic and GC7-driven inhibition of eIF5A^{H} silences mitochondria in kidney cells, preventing anoxic cell death and improving kidney transplant outcome (Melis et al., 2017). Our observations suggest that the MTS we identified as having an increased

(B) ^{13}C-Arginine trace analysis in M0, M(LPS), M(L/γ), and M(IL-4). Cells were polarized overnight in SILAC media containing 1.1 mM ^{13}C arginine ± 2.5 mM DFMO.
(C) Expression of macrophage alternative activation markers assessed by flow cytometry in BMMφ exposed to IL-4 ± 500 nM rotenone (complex I inhibitor) or 5 μM antimycin A (complex III inhibitor) or 200 nM myxothiazol (complex III inhibitor) or 5 μM oligomycin (complex V inhibitor) for 20 h (n = 7).
(D) CD301 and RELMα expression assayed by flow cytometry in M(IL-4) treated with 10 μM GC7 or 20 μM CPX for 24 h.
(E) Expression of human macrophage alternative activation markers assessed by flow cytometry in human monocyte-derived macrophages exposed to IL-4 ± 10 μM GC7 for 20 h (n = 3 individual donors).
(F) C57BL/6 mice were administered IL-4:αIL-4 complex at 5:25 μg by intraperitoneal (i.p.) injection. 24 h later eIF5A and eIF5A^{H} levels were assessed by flow cytometry in peritoneal macrophages (Ly6G^{-} Ly6C^{-} Siglec-F^{-} F4/80^{hi} CD11b^{+}) (n = 5 per group).
(G) Absolute number of peritoneal macrophages elicited from mice treated with IL-4:αIL-4 complex at 5:25 μg on days 2 and 4 ± 10 mg/kg GC7 on days 0–3 (n = 4–5 per group).
(H) C57BL/6 mice were treated with IL-4:αIL-4 complex by i.p. injection at 5:25 μg on days −4, −2, and day 0 ± 10 mg/kg GC7 on days −4 to 0. On day 0, mice were orally infected with *H. polygyrus* by gavage and absolute counts of peritoneal macrophages and intestinal worm burden were assessed on day 15 post-infection (∅ = naive control) (n = 6 per group).
(I) Mice were treated with 8 mg/kg LPS ± 10 mg/kg GC7 by i.p. injection, 12-h later serum IL-12 and IL-6 levels were quantified, as were markers of classical macrophage activation in peritoneal macrophages (Ly6G^{-} Ly6C^{-} Siglec-F^{-} F4/80^{hi} CD11b^{+}) measured by flow cytometry (n = 5 per group). All data are means ± SEM ($p^{*} < 0.05$, $p^{**} < 0.005$, compared with M(IL-4) condition, or IL-4c). (A) Representative of three individual mice and two experiments, (B, C, G, and I) of two experiments, (D) of three experiments, and (E, H) of one experiment.

dependency on eIF5A^{H} were expressed less efficiently, denoted by their decreased mCherry expression. These results suggested to us that the selectivity of enhanced eIF5A^{H} dependency, at least in one aspect, might be at the level of translational efficiency. Precisely how eIF5A^{H} mediates this effect is not known. Interestingly, eIF5A has been shown to copurify with mitochondrial proteins (Pereira et al., 2016), but how the potential mitochondrial targeting of eIF5A might influence our results here is not clear.

Both polyamine synthesis and eIF5A expression are augmented in cancer cells (Casero and Marton, 2007; Mathews and Hershey, 2015). Although these changes were largely thought to be important for driving proliferation, our data suggest tha these alterations might also affect mitochondrial activity in cancer cells. Previous studies have also demonstrated the engagement of polyamine biosynthesis and eIF5A in immune cells (Bevec et al., 1994; Hukelmann et al., 2016; Wang et al., 2011), and we believe our results here highlight an important function of this pathway in controlling OXPHOS. In line with previous reports (Huang et al., 2014; Van den Bossche et al., 2016; Vats et al., 2006), we confirm an important role for OXPHOS in macrophage alternative activation. Recent analysis of alternative activation at the mRNA level during ETC complex inhibition suggested that OXPHOS was dispensable for M(IL-4) (Divakaruni et al., 2018), these observations might imply that OXPHOS regulates M(IL-4) activation in a post-transcriptional manner. At the outset of our study we viewed this pathway to control mitochondrial metabolism, one that may remain on in the basal state, but could also be dynamically regulated to ramp up or down, depending on activation state and needs of the cell. However, our data showing that M0 macrophages have much less eIF5A^{H} than M(IL-4) macrophages at 4, 12, or 24 h after activation suggest that this is not the case, as both cell types seem to have similar expression of mitochondrial enzymes we identify as having an enhanced dependency on eIF5A^{H}. Nevertheless, M(IL-4) have higher respiration rates than M0, perhaps suggesting that eIF5A^{H} has additional effects on other proteins that promote TCA flux and OXPHOS. Indeed, our proteomics study revealed 90 proteins that were hyperdependent on eIF5A^{H}, but were not mitochondrial proteins. More work is needed to determine the full scope of how hypusine and eIF5A influences mitochondrial activity in these cells.

Our data suggested that, at least for the few MTS we studied, sequence-specific properties conferred increased dependency on eIF5AH. Given that the SV40 NLS, which is rich in positively charged residues, is not subject to eIF5A^{H} regulation in this study, it is unlikely that the presence of positively charged residues alone confers specificity. Recent evidence notes that the location of these residues may play a role in regulation by eIF5A^{H}, suggesting that MTS secondary structure or other elements may influence ribosome stalling and hence reliance on eIF5A^{H} (Pelechano and Alepuz, 2017; Schuller et al., 2017). The precise nature of the sequence-specific properties, or any potential structural differences in MTS, or how additional factors modulate the ultimate effect eIF5A^{H} has on their translation, has yet to be determined.

We remain interested in the upstream signals that influence the polyamine-eIF5A^{H} pathway in immune cells. We speculate that the enrichment of eIF5A^{H} in M(IL-4) is driven by an upturn in substrate abundance. Increased ornithine in M(IL-4) due to upregulated arginase expression results in enhanced substrate for ODC to generate putrescine, and ultimately spermidine, which can be used to synthesize hypusine. A scenario such as this may mean that, even if expression of polyamine-hypusine enzymes is not altered, hypusine synthesis can be augmented because of increased ornithine, putrescine, and spermidine availability. Overall, our data suggest that arginase expression during macrophage alternative activation serves to promote hypusination to support mitochondrial metabolism.

Arginase is expressed in several immune cell types (Bando et al., 2013; Monticelli et al., 2016; Pesce et al., 2009), and its expression in macrophages leads to the breakdown of arginine, which acts to deplete arginine from the extracellular environment and thereby inhibit the activation of T cells that depend on this amino acid substrate (Rodríguez et al., 2004). Since it is known that polyamines are important for cell proliferation, it is possible that cells that deplete arginine, something that cancer cells also do to support their own proliferation, block polyamine biosynthesis in T cells, thereby inhibiting their proliferation. More work will need to be done to determine how upstream substrates such as ornithine influence eIF5A^{H} in immune cells and whether this ultimately influences their function.

Limitations of Study

While our study shows that the polyamine-eIF5A-hypusine axis influences the TCA cycle and mitochondrial respiration, and thus controls macrophage activation, a full understanding of how eIF5A^{H} affects the expression of specific proteins, and in particular certain MTS, remains to be determined. Our experiments do not delineate whether eIF5A^{H} directly effects translation of certain transcripts, or whether it acts through an indirect mechanism that ultimately affects the expression of certain proteins.

STAR★METHODS

Detailed methods are provided in the online version of this paper and include the following:

- KEY RESOURCES TABLE
- CONTACT FOR REAGENT AND RESOURCE SHARING
- EXPERIMENTAL MODEL DETAILS
  - Mice and Immunizations
  - Cell Culture
- METHOD DETAILS
  - Metabolic Profiling
  - Western Blot
  - Retroviral Transduction
  - Lentiviral Transductions
  - siRNA Knockdown of *Eif5a* and *Dhps* in MEFS
  - Proteomics
  - Flow Cytometry and Confocal Microscopy
  - RT-PCR
  - Polysome Profile Analysis
- QUANTIFICATION AND STATISTICAL ANALYSIS
- DATA AND SOFTWARE AVAILABILITY

SUPPLEMENTAL INFORMATION

Supplemental Information can be found online at https://doi.org/10.1016/j.cmet.2019.05.003.

ACKNOWLEDGMENTS

We thank Katja Simon for her assistance with *in vivo* experiments, Asifa Akhtar and Adam Karoutas for cell lines, and Stephan Ehl for providing access to human samples. The work was supported by a Sir Henry Wellcome Fellowship awarded by the Wellcome Trust to D.J.P.; Alexander Von Humboldt Foundation Fellowships to A.M.K., M.V., and M.C.; a Swiss National Science Foundation Fellowship to M.M.; NIH grant HL11879 to B.R.B.; Deutsche Forschungsgemeinschaft (DFG RO 1028/5-2) and Excellence Initiative of the German federal and state governments (BIOSS-2) to S.R.; NIH grant AI110481 to E.J.P.; Swiss National Science Foundation grant 31003A 150066 to S.B.; NIH grant CA18125 to E.L.P.; and by the Max Planck Society.

AUTHOR CONTRIBUTIONS

D.J.P., M.D.B., R.I.K.G., S.R., B.R.B., D.Z., E.J.P., S.B., and E.L.P. designed the research, provided conceptual input, and analyzed the data. D.J.P., M.D.B., R.I.K.G., R.L.K., A.M.C., A.C., A.M.K., J.Q., A.E.P., S.S., F.A., S.K.A., B.K., K.M.G., M.V., M.C., N.P., Y.M., G.C., C.S.F., L.J.F., M.M., D.O., J.D.C., Y.Z., F.B., M.E.M., K.P., D.E.S., G.M., and J.M.B. performed the experiments. D.J.P. and E.L.P. wrote the manuscript.

DECLARATION OF INTERESTS

D.J.P. and E.L.P. have filed a provisional patent application: modulating activation of macrophages (M2 cells) through the polyamine-eIF5A-hypusine axis. E.L.P is a SAB member of ImmunoMet and a founder of Rheos Medicines. E.J.P. is a founder of Rheos Medicines.

Received: January 31, 2019
Revised: April 5, 2019
Accepted: April 30, 2019
Published: May 23, 2019

REFERENCES

Abbruzzese, A., Park, M.H., and Folk, J.E. (1986). Deoxyhypusine hydroxylase from rat testis. Partial purification and characterization. J. Biol. Chem. *261*, 3085–3089.

Arpa, L., Valledor, A.F., Lloberas, J., and Celada, A. (2009). IL-4 blocks M-CSF-dependent macrophage proliferation by inducing p21WAF1 in a STAT6-dependent way. Eur. J. Immunol. *39*, 514–526.

Bando, J.K., Nussbaum, J.C., Liang, H.E., and Locksley, R.M. (2013). Type 2 innate lymphoid cells constitutively express arginase-I in the naive and inflamed lung. J. Leukoc. Biol. *94*, 877–884.

Bevec, D., Klier, H., Holter, W., Tschachler, E., Valent, P., Lottspeich, F., Baumruker, T., and Hauber, J. (1994). Induced gene expression of the hypusine-containing protein eukaryotic initiation factor 5A in activated human T lymphocytes. Proc. Natl. Acad. Sci. USA *91*, 10829–10833.

Buck, M.D., Sowell, R.T., Kaech, S.M., and Pearce, E.L. (2017). Metabolic instruction of immunity. Cell *169*, 570–586.

Buescher, J.M., Antoniewicz, M.R., Boros, L.G., Burgess, S.C., Brunengraber, H., Clish, C.B., DeBerardinis, R.J., Feron, O., Frezza, C., Ghesquiere, B., et al. (2015). A roadmap for interpreting (13) C metabolite labeling patterns from cells. Curr. Opin. Biotechnol. *34*, 189–201.

Casero, R.A., and Marton, L.J. (2007). Targeting polyamine metabolism and function in cancer and other hyperproliferative diseases. Nat. Rev. Drug Discov. *6*, 373–390.

Chang, C.H., Qiu, J., O'Sullivan, D., Buck, M.D., Noguchi, T., Curtis, J.D., Chen, Q., Gindin, M., Gubin, M.M., van der Windt, G.J.W., et al. (2015). Metabolic competition in the tumor microenvironment is a driver of cancer progression. Cell *162*, 1229–1241.

Charneski, C.A., and Hurst, L.D. (2013). Positively charged residues are the major determinants of ribosomal velocity. PLoS Biol. *11*, e1001508.

Cox, J., Hein, M.Y., Luber, C.A., Paron, I., Nagaraj, N., and Mann, M. (2014). Accurate proteome-wide label-free quantification by delayed normalization and maximal peptide ratio extraction, termed MaxLFQ. Mol. Cell Proteomics *13*, 2513–2526.

Cox, J., and Mann, M. (2008). MaxQuant enables high peptide identification rates, individualized p.p.b.-range mass accuracies and proteome-wide protein quantification. Nat. Biotechnol. *26*, 1367–1372.

Cox, J., Neuhauser, N., Michalski, A., Scheltema, R.A., Olsen, J.V., and Mann, M. (2011). Andromeda: a peptide search engine integrated into the MaxQuant environment. J. Proteome Res. *10*, 1794–1805.

Divakaruni, A.S., Hsieh, W.Y., Minarrieta, L., Duong, T.N., Kim, K.K.O., Desousa, B.R., Andreyev, A.Y., Bowman, C.E., Caradonna, K., Dranka, B.P., et al. (2018). Etomoxir inhibits macrophage polarization by disrupting CoA homeostasis. Cell Metab *28*, 490–503.e7.

Eisenberg, T., Knauer, H., Schauer, A., Büttner, S., Ruckenstuhl, C., Carmona-Gutierrez, D., Ring, J., Schroeder, S., Magnes, C., Antonacci, L., et al. (2009). Induction of autophagy by spermidine promotes longevity. Nat. Cell Biol. *11*, 1305–1314.

Engelke, R., Riede, J., Hegermann, J., Wuerch, A., Eimer, S., Dengjel, J., and Mittler, G. (2014). The quantitative nuclear matrix proteome as a biochemical snapshot of nuclear organization. J. Proteome Res. *13*, 3940–3956.

Gutierrez, E., Shin, B.S., Woolstenhulme, C.J., Kim, J.R., Saini, P., Buskirk, A.R., and Dever, T.E. (2013). eIF5A promotes translation of polyproline motifs. Mol. Cell *51*, 35–45.

Henderson, A., and Hershey, J.W. (2011). Eukaryotic translation initiation factor (eIF) 5A stimulates protein synthesis in Saccharomyces cerevisiae. Proc. Natl. Acad. Sci. USA *108*, 6415–6419.

Heyer, E.E., and Moore, M.J. (2016). Redefining the translational status of 80S monosomes. Cell *164*, 757–769.

Hoque, M., Hanauske-Abel, H.M., Palumbo, P., Saxena, D., Gandolfi, D.D., Pe'ery, T., Mathews, M.B., and Park, M.H. (2009). Inhibition of HIV-1 gene expression by Ciclopirox and Deferiprone, drugs that prevent hypusination of eukaryotic initiation factor 5A. Retrovirology, 6–90.

Huang, S.C.-c., Everts, B., Ivanova, Y., O'Sullivan, D., Nascimento, M., Smith, A.M., Beatty, W., Love-Gregory, L., Lam, W.Y., O'Neil, C.M., et al. (2014). Cell-intrinsic lysosomal lipolysis is essential for alternative activation of macrophages. Nat. Immunol. *15*, 846–855.

Hukelmann, J.L., Anderson, K.E., Sinclair, L.V., Grzes, K.M., Murillo, A.B., Hawkins, P.T., Stephens, L.R., Lamond, A.I., and Cantrell, D.A. (2016). The cytotoxic T cell proteome and its shaping by the kinase mTOR. Nat. Immunol. *17*, 104–112.

Jaiswal, H., Conz, C., Otto, H., Wölfle, T., Fitzke, E., Mayer, M.P., and Rospert, S. (2011). The chaperone network connected to human ribosome-associated complex. Mol. Cell. Biol. *31*, 1160–1173.

Jenkins, S.J., Ruckerl, D., Cook, P.C., Jones, L.H., Finkelman, F.D., Van Rooijen, N., MacDonald, A.S., and Allen, J.E. (2011). Local macrophage proliferation, rather than recruitment from the blood, is a signature of TH2 inflammation. Science *332*, 1284–1288.

Jenkins, Z.A., Hååg, P.G., and Johansson, H.E. (2001). Human EIF5A2 on chromosome 3q25-q27 is a phylogenetically conserved vertebrate variant of eukaryotic translation initiation factor 5A with tissue-specific expression. Genomics *71*, 101–109.

Kang, H.A., and Hershey, J.W. (1994). Effect of initiation-factor Eif-5a depletion on protein-synthesis and proliferation of Saccharomyces-cerevisiae. J. Biol. Chem. *269*, 3934–3940.

Kelly, S.M., Vanslyke, J.K., and Musil, L.S. (2007). Regulation of ubiquitin-proteasome system mediated degradation by cytosolic stress. Mol. Biol. Cell *18*, 4279–4291.

Kelstrup, C.D., Young, C., Lavallee, R., Nielsen, M.L., and Olsen, J.V. (2012). Optimized fast and sensitive acquisition methods for shotgun proteomics on a quadrupole Orbitrap mass spectrometer. J. Proteome Res. *11*, 3487–3497.

Kulak, N.A., Pichler, G., Paron, I., Nagaraj, N., and Mann, M. (2014). Minimal, encapsulated proteomic-sample processing applied to copy-number estimation in eukaryotic cells. Nat. Methods *11*, 319–324.

Liu, L., Lu, Y., Martinez, J., Bi, Y., Lian, G., Wang, T., Milasta, S., Wang, J., Yang, M., Liu, G., et al. (2016). Proinflammatory signal suppresses proliferation and shifts macrophage metabolism from Myc-dependent to HIF1α-dependent. Proc. Natl. Acad. Sci. USA *113*, 1564–1569.

Lubas, M., Harder, L.M., Kumsta, C., Tiessen, I., Hansen, M., Andersen, J.S., Lund, A.H., and Frankel, L.B. (2018). eIF5A is required for autophagy by mediating ATG3 translation. EMBO Rep. *19*, e46072.

Mathews, M.B., and Hershey, J.W.B. (2015). The translation factor eIF5A and human cancer. Biochim. Biophys. Acta *1849*, 836–844.

Melis, N., Rubera, I., Cougnon, M., Giraud, S., Mograbi, B., Belaid, A., Pisani, D.F., Huber, S.M., Lacas-Gervais, S., Fragaki, K., et al. (2017). Targeting eIF5A hypusination prevents anoxic cell death through mitochondrial silencing and improves kidney transplant outcome. J. Am. Soc. Nephrol. *28*, 811–822.

Miller-Fleming, L., Olin-Sandoval, V., Campbell, K., and Ralser, M. (2015). Remaining mysteries of molecular biology: the role of polyamines in the cell. J. Mol. Biol. *427*, 3389–3406.

Monticelli, L.A., Buck, M.D., Flamar, A.L., Saenz, S.A., Tait Wojno, E.D.T., Yudanin, N.A., Osborne, L.C., Hepworth, M.R., Tran, S.V., Rodewald, H.R., et al. (2016). Arginase 1 is an innate lymphoid-cell-intrinsic metabolic checkpoint controlling type 2 inflammation. Nat. Immunol. *17*, 656–665.

Nakanishi, S., and Cleveland, J.L. (2016). Targeting the polyamine-hypusine circuit for the prevention and treatment of cancer. Amino Acids *48*, 2353–2362.

Nishiki, Y., Farb, T.B., Friedrich, J., Bokvist, K., Mirmira, R.G., and Maier, B. (2013). Characterization of a novel polyclonal anti-hypusine antibody. SpringerPlus *2*, 421.

Pällmann, N., Braig, M., Sievert, H., Preukschas, M., Hermans-Borgmeyer, I., Schweizer, M., Nagel, C.H., Neumann, M., Wild, P., Haralambieva, E., et al. (2015). Biological relevance and therapeutic potential of the hypusine modification system. J. Biol. Chem. *290*, 18343–18360.

Park, M.H., Cooper, H.L., and Folk, J.E. (1981). Identification of hypusine, an unusual amino-acid, in a protein from human-lymphocytes and of spermidine as its biosynthetic precursor. Proc. Natl. Acad. Sci. USA *78*, 2869–2873.

Pegg, A.E. (2016). Functions of polyamines in mammals. J. Biol. Chem. *291*, 14904–14912.

Pelechano, V., and Alepuz, P. (2017). eIF5A facilitates translation termination globally and promotes the elongation of many non polyproline-specific tripeptide sequences. Nucleic Acids Res. *45*, 7326–7338.

Pereira, K.D., Tamborlin, L., Meneguello, L., de Proença, A.R.G., Almeida, I.C.A., Lourenço, R.F., and Luchessi, A.D. (2016). Alternative start codon connects eIF5A to mitochondria. J. Cell. Physiol. *231*, 2682–2689.

Pesce, J.T., Ramalingam, T.R., Mentink-Kane, M.M., Wilson, M.S., El Kasmi, K.C., Smith, A.M., Thompson, R.W., Cheever, A.W., Murray, P.J., and Wynn, T.A. (2009). Arginase-1-expressing macrophages suppress Th2 cytokine-driven inflammation and fibrosis. PLoS Pathog. *5*, e1000371.

Pickles, S., Vigié, P., and Youle, R.J. (2018). Mitophagy and quality control mechanisms in mitochondrial maintenance. Curr. Biol. *28*, R170–R185.

Poulin, R., Lu, L., Ackermann, B., Bey, P., and Pegg, A.E. (1992). Mechanism of the irreversible inactivation of mouse ornithine decarboxylase by alpha-difluoromethylornithine. Characterization of sequences at the inhibitor and coenzyme binding-sites. J. Biol. Chem. *267*, 150–158.

Preukschas, M., Hagel, C., Schulte, A., Weber, K., Lamszus, K., Sievert, H., Pällmann, N., Bokemeyer, C., Hauber, J., Braig, M., et al. (2012). Expression of eukaryotic initiation factor 5A and hypusine forming enzymes in glioblastoma patient samples: implications for new targeted therapies. PLoS One *7*, e43468.

Rodríguez, P.C., Quiceno, D.G., Zabaleta, J., Ortiz, B., Zea, A.H., Piazuelo, M.B., Delgado, A., Correa, P., Brayer, J., Sotomayor, E.M., et al. (2004). Arginase I production in the tumor microenvironment by mature myeloid cells inhibits T-cell receptor expression and antigen-specific T-cell responses. Cancer Res. *64*, 5839–5849.

Sabi, R., and Tuller, T. (2015). A comparative genomics study on the effect of individual amino acids on ribosome stalling. BMC Genomics *16*.

Saini, P., Eyler, D.E., Green, R., and Dever, T.E. (2009). Hypusine-containing protein eIF5A promotes translation elongation. Nature *459*, 118–121.

Schuller, A.P., Wu, C.C.-c., Dever, T.E., Buskirk, A.R., and Green, R. (2017). eIF5A functions globally in translation elongation and termination. Mol. Cell *66*, 194–205.e5.

Stanić, I., Facchini, A., Borzì, R.M., Stefanelli, C., and Flamigni, F. (2009). The polyamine analogue N1,N11-diethylnorspermine can induce chondrocyte apoptosis independently of its ability to alter metabolism and levels of natural polyamines. J. Cell. Physiol. *219*, 109–116.

Tannahill, G.M., Curtis, A.M., Adamik, J., Palsson-McDermott, E.M., McGettrick, A.F., Goel, G., Frezza, C., Bernard, N.J., Kelly, B., Foley, N.H., et al. (2013). Succinate is an inflammatory signal that induces IL-1β through HIF-1α. Nature *496*, 238–242.

Thomas, T., and Thomas, T.J. (2001). Polyamines in cell growth and cell death: molecular mechanisms and therapeutic applications. Cell. Mol. Life Sci. *58*, 244–258.

Tyanova, S., Temu, T., Sinitcyn, P., Carlson, A., Hein, M.Y., Geiger, T., Mann, M., and Cox, J. (2016). The Perseus computational platform for comprehensive analysis of (prote)omics data. Nat. Methods *13*, 731–740.

Van den Bossche, J., Baardman, J., Otto, N.A., van der Velden, S., Neele, A.E., van den Berg, S.M., Luque-Martin, R., Chen, H.J., Boshuizen, M.C.S., Ahmed, M., et al. (2016). Mitochondrial dysfunction prevents repolarization of inflammatory macrophages. Cell Rep. *17*, 684–696.

Van Der Kelen, K., Beyaert, R., Inzé, D., and De Veylder, L. (2009). Translational control of eukaryotic gene expression. Crit. Rev. Biochem. Mol. Biol. *44*, 143–168.

Vats, D., Mukundan, L., Odegaard, J.I., Zhang, L., Smith, K.L., Morel, C.R., Wagner, R.A., Greaves, D.R., Murray, P.J., and Chawla, A. (2006). Oxidative metabolism and PGC-1beta attenuate macrophage-mediated inflammation. Cell Metab. *4*, 13–24.

Wang, R., Dillon, C.P., Shi, L.Z., Milasta, S., Carter, R., Finkelstein, D., McCormick, L.L., Fitzgerald, P., Chi, H., Munger, J., et al. (2011). The transcription factor Myc controls metabolic reprogramming upon T lymphocyte activation. Immunity *35*, 871–882.

Wolff, E.C., Lee, Y.B., Chung, S.I., Folk, J.E., and Park, M.H. (1995). Deoxyhypusine synthase from rat testis: purification and characterization. J. Biol. Chem. *270*, 8660–8666.

STAR★METHODS

KEY RESOURCES TABLE

REAGENT or RESOURCE	SOURCE	IDENTIFIER
Antibodies		
Anti-Hypusine	Millipore,	Polyclonal, ABS1064
Anti-eif5a	BD Biosciences	26/eIF-5a
Anti-GAPDH	Cell Signaling,	D16H11
Anti- alpha tubulin	Sigma	DM1A
Anti-rabbit DHPS	Abcam	Polyclonal, ab190266
Anti- hexokinase II	Cell signaling	C64G5
Anti- IDH2	Cell signaling	D7H6Q
Anti- DLD (lipoamide dehydrogenase)	Abcam,	EPR6635
Anti- SUCLG1 (succinyl CoA Synthetase)	Cell Signaling	Polyclonal, 5557
Anti- SDHA (succinate dehydrogenase A)	Cell Signaling	D6J9M
Anti- SDHB (Succinate dehydrogenase B)	Abcam	21A11AE7
Anti- methylmalonyl coA mutase	Abcam	EPR7738
Anti- rodent oxphos cocktail	Abcam	Monoclonal mix, ab110413
Anti- citrate synthase	Cell signaling	D7V8B
Anti- IDH2	Cell Signaling	D7H6Q
Anti- MDH2 (malate dehydrogenase 2)	Cell signaling	D8Q5S
Anti- DOHH	Abcam	Polyclonal, ab122946
Anti-PDH (pyruvate dehydrogenase)	Cell signaling	C54G1
Anti-GLDH (glutamate dehydrogenase	Cell signaling	D9F7P
Anti-ABAT (4-aminobutyrate aminotransferase)	Abcam	EPR4433
Anti-ASL (argininosuccinate lyase)	Abcam	EPR19396
Anti-ACL (Acetyl CoA Carboxylase)	Cell signaling	C83B10
Anti-FAS (fatty acid synthase)	Cell signaling	C20G5
Anti-G6PDH (glucose-6-phosphate 1-dehydrogenase)	Cell Signaling	Polyclonal, 8866
Anti-hexokinase I	Cell signaling	C35C4
Anti-aconitase	Abcam	EPR7225
Anti-IDH1	Cell signalling	D2H1
Ant-LC3	Sigma	Polyclonal, L7543
Anti-ODC	Abcam	EPR5724
Anti-p-STAT6	Cell Signaling	Polyclonal, 9361
Anti-COX2	Cell Signaling	D5H5
Anti-NOS2	Santa Cruz	C-11
Anti-CD206	Biolegend	C068C2
Anti-CD301	Biorad/Biolegend	ER-MP23 and LOM-14
Anti-arginase I	eBioscience	AlexF5
Anti-RELM alpha	Peprotech	polyclonal
Anti-F4/80	Biolegend	BM8
Anti-CD11b	Biolegend/BD	M1/70
Anti-cd86	Biolegend	GL-1

(*Continued on next page*)

Continued

REAGENT or RESOURCE	SOURCE	IDENTIFIER
Anti-I-A/I-E (MHC Class II)	Biolegend/eBioscience	M5/114.15.2
Anti-human CD16	Biolegend	Clone: 3G8
Anti-human CD71	Biolegend	CY1G4
Anti-human CD206	eBioscience/Biolegend	19.2(eBioscience) 15-2 (Biolegend)
Anti-human CD209	BD/Biolegend	DCN46(BD) 9E9A8 (biolegend)
Biological Samples		
Blood from healthy human donors	University of Freiburg	CCI Biometric Bank (IRB approval No. 282/11
Chemicals, Peptides, and Recombinant Proteins		
N^1,N^{11}-Diethylnorspermine tetrahydrochloride	Tocris	6618
DFMO	Enzo Life Sciences	ALX-270-283-M050
GC7	Millipore	259545
Ciclopirox	Sigma	SML2011
IPTG	Sigma	I6758
4-OHT	Sigma	T5648
Rotenone	Sigma	R8875
Antimycin A	Sigma	A8674
Myxothiazol	Sigma	T5580
Oligomycin	Sigma	O4876
2-Deoxyglucose	Alfa Aesar	L07338
FCCP	Sigma	C2920
Bafilomycin A1	Alfa Aesar	J61835
Succinate	Sigma	S9637
Near IR Live-Dead fixable	Thermo	Catalogue No: L10119
Live/Dead Fixable Violet	Thermo	L34955
C13 Glucose	Cambridge Isoptope laboratories	CLM-1396
C13 Glutamine	Cambridge Isoptope laboratories	DML-1826
C13 Palmitate	Cambridge Isoptope laboratories	CLM-409
Mouse Recombinant IFNgamma	Peprotech	315-05
Mouse recombinant IL-4	Peprotech	214–14
Mouse recombinant M-CSF	Peprotech	315-02
Human recombinant M-CSF	R&D Systems	216-MC-500
Human recombinant IL-4	R&D Systems	204-IL-050
RMPI	Thermo	21875158
DMEM	Thermo	31885049
FCS	Thermo	10099141
Glutamine	Thermo	25030-024
LPS	Sigma	L4391
Critical Commercial Assays		
IL-6	Biolegend	431303
IL-12 ELISA	Biolegend	431602

(*Continued on next page*)

Continued

REAGENT or RESOURCE	SOURCE	IDENTIFIER
Deposited Data		
Proteomics Data	ProteomeXchange Consortium via PRIDE repository	PXD013443
Experimental Models: Cell Lines		
NIH3T3	ATCC	CRL-1658
EG7-OVA	ATCC	CRL-2113
Eif5a-shRNA-expressing NIH3T3 MEFs	Gift from Dr Stefan Balabanov	NA
$Dhps^{flox/flox}$ ERT2-Cre MEFs	Pällmann et al., 2015	NA
Experimental Models: Organisms and Strains		
C57BL/6J mice	Jackson Labs.	000664
YARG	Jackson Labs	015857
Oligonucleotides		
Taqman primers: Citrate synthase (Cs)	Applied Biosystems	4331182/Mm00466043_m1
Taqman primers: Dld	Applied Biosystems	4331182 /Mm00432831_m1
Taqman primers: Suclg1	Applied Biosystems	4448892/Mm00451244_m1
Taqman primers: Sdha	Applied Biosystems	4331182/ Mm01352366_m1
Taqman primers: Mdh2	Applied Biosystems	4331182/ Mm00725890_s1
Taqman primers Mut	Applied Biosystems	4331182 /Mm00485312_m1
Taqman primers: Idh2	Applied Biosystems	4331182 /Mm00612429_m1
Taqman primers: gapdh	Applied Biosystems	4331182 /Mm99999915_g1
Recombinant DNA		
MSCV-LTRmiR30-PIG (LMP) For hp constructs		Addgene plasmid #24071
MSCV-I-GFP (MIGR1) For MTS constructs		Addgene plasmid #27490
LMP-control hp	Open Biosystems	Addgene plasmid #24071
LMP-EIF5a hp Black: 5' miR30 context Blue: EIF5a sense sequence Green: Loop Red: EIF5a antisense sequence Black: 3' miR30 context	Sigma	TGCTGTTGACAGTGAGCGCCCATGAA GATATCTGCCCGTCAATAGTGAAGCC ACAGATGTATTGACGGGCAGATATCT TCATAGTTGCCTACTGCCTCGGA
LMP-Dhps hp Black: 5' miR30 context Blue: Dhps sense sequence Green: Loop Red: Dhps antisense sequence Black: 3' miR30 context	Sigma	TGCTGTTGACAGTGAGCGCCCACATC CCTGTGCTGAGTCCATAGTGAAGCCA CAGATGTATGGACTCAGCACAGGGAT GGTTGCCTACTGCCTCGGA
LMP-Dohh hp Black: 5' miR30 context Blue: Dohh sense sequence Green: Loop Red: Dohh antisense sequence Black: 3' miR30 context	Sigma	TGCTGTTGACAGTGAGCGCCCGTGCTG CATGAATAAAATATAGTGAAGCCACAG ATGTATATTTTATTCATGCAGCACGGTT GCCTACTGCCTCGGA

(*Continued on next page*)

Continued

REAGENT or RESOURCE	SOURCE	IDENTIFIER
mcs-GSGSG-mCherryDEG Black: multiple cloning site (**XhoI-BamHI**) Yellow: **BamHI site** GSGSG linker Red: mCherry Green: ODC degron **Black: EcoRI cloning site**	IDT	**CTCGAG**CCAACT**GGATCC**GGCTCCGG CTCCGGAGTGAGCAAGGGCGAGGAGG ATAACATGGCCATCATCAAGGAGTTCA TGCGCTTCAAGGTGCACATGGAGGGCT CCGTGAACGGCCACGAGTTCGAGATCG AGGGCGAGGGCGAGGGCCGCCCCTAC GAGGGCACCCAGACCGCCAAGCTGAA GGTGACCAAGGGTGGCCCCCTGCCCT TCGCCTGGGACATCCTGTCCCCTCAG TTCATGTACGGCTCCAAGGCCTACGT GAAGCACCCCGCCGACATCCCCGACT ACTTGAAGCTGTCCTTCCCCGAGGGC TTCAAGTGGGAGCGCGTGATGAACTT CGAGGACGGCGGCGTGGTGACCGTG ACCCAGGACTCCTCCCTGCAGGACGG CGAGTTCATCTACAAGGTGAAGCTGCG CGGCACCAACTTCCCCTCCGACGGCCC CGTAATGCAGAAGAAGACGATGGGCTG GGAGGCCTCCTCCGAGCGGATGTACCC CGAGGACGGCGCCCTGAAGGGCGAGAT CAAGCAGAGGCTGAAGCTGAAGGACGG CGGCCACTACGACGCTGAGGTCAAGAC CACCTACAAGGCCAAGAAGCCCGTGCA GCTGCCCGGCGCCTACAACGTCAACATC AAGTTGGACATCACCTCCCACAACGAGG ACTACACCATCGTGGAACAGTACGAACG CGCCGAGGGCCGCCACTCCACCGGCGG CATGGACGAGCTGTACAAGCATGGCTT CCCGCCGGAGGTGGAGGAGCAGGATG ATGGCACGCTGCCCATGTCTTGTGCCCA GGAGAGCGGGATGGACCGTCACTAA**GAATTC**
SV40 NLS **Red: XhoI site** Blue: SV40 NLS (MPKKKRKV) **Yellow: BamHI site**	IDT	**CTCGAG**ATGCCTAAAAAGAAGAGGAA GGTA**GGATCC**G
SUCLG1 MTS **Red: XhoI site** Blue: SUCLG1 MTS (MTATVVAAAATATMVSSSSGL AAARLLSRTFLLQQNGIRHG) **Yellow: BamHI site**	IDT	**CTCGAG**ATGACCGCAACAGTAGTTGCTGCG GCTGCCACTGCAACCATGGTCTCCAGCAGC AGCGGCCTCGCCGCCGCCCGCCTGTTGTCG CGCACCTTCCTCCTGCAACAGAATGGGATA CGACACGGG**GGATCC**
SDHA MTS **Red: XhoI site** Blue: SDHA MTS (MAGVGAVSRLLRGRRLALTGAWPGTLQK QTCGFHFSVGENKKASAKVSDAISTQYPVVD) **Yellow: BamHI site**	IDT	**CTCGAG**ATGGCCGGGGTTGGCGCAGTTTC GAGGCTTCTTCGCGGGCGGCGCTTGGCG TTAACTGGGGCGTGGCCAGGAACACTCCA AAAACAGACCTGCGGCTTTCACTTCTCTG TTGGTGAGAACAAGAAGGCATCAGCTAAA GTTTCAGATGCAATTTCTACTCAATACCCA GTGGTGGAT**GGATCC**
IDH2 MTS **Red: XhoI site** Blue: IDH2 MTS (MAGYLRAVSSLCRASG SARTWAPAALTVPSWPEQPRRHY) **Yellow: BamHI site**	IDT	**CTCGAG**ATGGCCGGCTACCTGCGGGCTGT GAGCTCGCTCTGCAGAGCCTCGGGCTCAG CGCGGACCTGGGCACCGGCAGCACTGACT GTCCCCAGCTGGCCGGAGCAGCCGCGGC GCCACTAT**GGATCC**
MCM MTS **Red: XhoI site** Blue: MCM MTS (MLRAKNQLFLLSPHYLK QLNIPSASRWKRLL) **Yellow: BamHI site**	IDT	**CTCGAG**ATGTTGAGAGCTAAGAATCAACTT TTTTTGCTATCGCCCCATTACCTGAAGCAG CTAAACATTCCATCAGCTTCCAGATGGAAA CGCCTTCTA**GGATCC**G

(*Continued on next page*)

Continued

REAGENT or RESOURCE	SOURCE	IDENTIFIER
N'IDH2:SUCLG1-C' MTS **Red: XhoI site** Blue: **IDH2**:SUCLG1 fusion MTS (**MAGYLRAVSSLCRASGSARTW**SSG LAAARLLSRTFLLQQNGIRHG) **Yellow: BamHI site**	IDT	**CTCGAG**ATGGCTGGGTACCTCCGCGCAGT CTCAAGTCTCTGCCGGGCAAGCGGCAGCG CCCGCACATGGTCTTCCGGTTTGGCTGCT GCTAGACTGCTTAGTCGCACTTTTCTCCTT CAGCAGAACGGTATTAGACACGGG**GGATCC**G
N'SUCLG1:IDH2-C' MTS **Red: XhoI site** Blue: **SUCLG1**:IDH2 fusion MTS (MTATVVAAAATATMVSSSSG**APAAL** **TVPSWPEQPRRHY**) **Yellow: BamHI site**	IDT	**CTCGAG**ATGACTGCAACCGTAGTAGCCGC AGCCGCCACAGCCACTATGGTATCCTCATC ATCAGGCGCCCCTGCAGCCCTGACAGTAC CATCATGGCCAGAACAGCCAAGGCGACATT AT**GGATCC**
Software and Algorithms		
maxLFQ algorithm	Cox et al., 2014	NA
MaxQuant	Cox and Mann, 2008; Cox et al., 2011	NA
Perseus platform	Tyanova et al., 2016	NA
FlowJo	TreeStar	NA
Prism	GraphPad	NA

CONTACT FOR REAGENT AND RESOURCE SHARING

Further information and requests for resources and reagents should be directed to and will be fulfilled by the Lead Contact, Erika Pearce (pearce@ie-freiburg.mpg.de).

EXPERIMENTAL MODEL DETAILS

Mice and Immunizations

C57BL/6 (Jax, 000664) and Arg1-YFP C57BL/6 (Jax, 015857) were purchased from Jackson Laboratories. All mice were bred and maintained under specific pathogen free conditions under protocols approved by the Animal Welfare Committee of the Max Planck Institute of Immunobiology and Epigenetics, Freiburg, Germany. Mice used in all *in vitro* and *in vivo* experiments were 6–10 weeks of age and were age/sex matched. For infection with *H. polygyrus bakeri*, mice were infected orally by gavage with 200 infective L3 stage larvae. At day 15 post infection, mice were sacrificed and parasite burdens were measured. To count worms, intestines were removed, opened longitudinally, and placed on to muslin cloth draped on top of a 50 ml tube filled with complete RPMI for 4 h at 37°C. Parasites migrated through the cloth into the tube and were recovered for counting on a dissecting microscope. Parasite eggs were enumerated by soaking feces collected from individual mice in water, then diluting the fecal slurry with saturated sodium chloride and counting under a microscope using a McMaster counting chamber. Long acting IL-4 complex (IL-4c) consisted of a 2:1 molar ratio of recombinant mouse IL-4 (Peprotech, London) and anti-IL-4 mAb (clone 11B11; BioXcell, NH) and was administered by i.p. injection at the times indicated in the figure legend. Each mouse received 5 μg of IL-4 and 25 μg of 11B11, ± 10 mg/kg GC7 (Millipore). PBS was used as a vehicle control. For *in vivo studies* with LPS we administered 8mg/kg LPS (Sigma) by i.p. injection ± 10 mg/kg GC7. IL-12 and IL-6 quantification was assessed by ELISA (eBioscience) as per the manufacturer's instructions on serum 3 hours after LPS injection.

Cell Culture

Bone marrow cells were differentiated for 7 days into bone marrow macrophages (BMMφ) by culturing in complete medium (RPMI 1640 media supplemented with 10% FCS, 2mM L-glutamine, 100 U/mL penicillin/streptomycin) with 20 ng/mL macrophage colony-stimulating factor (M-CSF; PeproTech). M(IL-4) were generated with 20 ng/mL IL-4 overnight from day 7 of culture; M(LPS/IFNγ) were generated with 20 ng/mL LPS (Sigma) and 50 ng/mL IFN-γ (R&D Systems) overnight from day 7 of culture. All drug treatments on BMMφ began from day 7 of culture. N1-guanyl-1 7-diaminoheptane (GC7; Enzo Life Sciences) and ciclopirox (Sigma) were typically used at 10 μM and 20 μM, respectively, unless otherwise stated. Difluoromethyl ornithine (DFMO) and diethylnorspermine (DENSPM; Tocris) were used at 2.5 mM and 50 μM, respectively. Dimethylsuccinate (Sigma) was used at 5mM. $DHPS^{Flox/Flox}$ Cre-ER MEFs,were cultured in complete DMEM (DMEM supplemented with 10% FCS, 2mM L-glutamine, 100 U/mL penicillin/streptomycin) and generated as previously described (Pällmann et al., 2015). Cre-ER expression was induced with 1 μM 4-OHT (Sigma) for the indicated time period. NIH3T3 MEFs (purchased from ATCC) stably transduced with Eif5a-shRNA were grown in complete DMEM and *Eif5a*-shRNA expression was induced with 100 μM isopropyl-β-D-1 thiogalactopyranoside (IPTG, Sigma) for the indicated period of time.

Madin-Darby Kidney Canine (MDCK) cells were grown in complete DMEM, as was the human breast adenocarcinoma line MCF-7 but with 0.01mg/ml recombinant human insulin. *D. melanogaster* Schneider 2 (S2) cells were cultured without CO_2 at 28°C in complete Schneider's Drosophila medium (Gibco; supplemented with 10% FCS, 50 U/mL penicillin/streptomycin, 25% conditioned complete Schneider's medium). To generate human macrophages, we negatively selected monocytes from blood using the manufacturers instructions (Stem Cell). All subjects gave written informed consent in accordance with the Declaration of Helsinki and the study was performed according to the CCI Biometric Bank (IRB approval No. 282/11). Monocytes were differentiated into macrophages with 100 ng/mL human M-CSF (R&D Systems) for 6 days in complete medium (RPMI 1640 media supplemented with 10% FCS, 2mM L-glutamine, 100 U/mL penicillin/streptomycin). On day 6, macrophages were polarised with 20 ng/mL human IL-4 (R&D Systems) and analysed the next day.

METHOD DETAILS

Metabolic Profiling

Extracellular acidification rate (ECAR) and oxygen consumption rate (OCR) were measured using the Seahorse XFe Bioanalyser (Seahorse Bioscience). $8x10^4$ BMMφ were added to sea horse 96 well plates on day 7 of culture and analysed in XF media (non-buffered RPMI 1640 containing 25 mM glucose, 2 mM L-glutamine, and 1 mM sodium pyruvate) the following day after cytokine and drug treatment. Prior to analysis, cells were incubated for a minimum of 45 minutes at 37°C in the absence of CO_2. OCR and ECAR were measured under basal conditions, or after the addition of the following drugs: 1 μM oligomycin, 1.5 μM fluoro-carbonyl cyanide phenylhydrazone (FCCP), 100 nM rotenone, and 1 μM antimycin A (all Sigma). Measurements were taken using a 96 well Extracellular Flux Analyser (Seahorse Bioscience).

Metabolite Tracing

BMMφ on day 7 of culture were washed and cultured in complete RPMI 1640 (minus glucose or glutamine), supplemented with either 11mM ^{13}C-glucose or 4mM ^{13}C-glutamine, for 24 hours. ^{13}C-palmitate (20 μM) was added to complete RMPI 1640 overnight. ^{13}C-Arginine tracing was performed by culturing cells in SILAC media supplemented with 0.2 mM L-lysine and 1.1 mM ^{13}C-Arginine for 24 hours. MEFs were washed and cultured in complete DMEM (with 10% dialysed serum, minus glucose or glutamine), supplemented with 25 mM ^{13}C-glucose or 4 mM ^{13}C-glutamine, for 24 hours. For harvest, cells were rinsed with cold 0.9% NaCl and metabolites extracted using 1.2 mL of 80% MeOH kept on dry ice. 10 nM norvaline (internal standard) was added. For putrescine detection, metabolites were extracted in 80% MeOH containing 3% formic acid. Following mixing and centrifugation, the supernatant was collected and dried via centrifugal evaporation. Dried metabolite extracts were resuspended in pyridine and derivatized with methoxyamine (sc-263468 Santa Cruz Bio) for 60 minutes at 37°C and subsequently with N-(tert-butyldimethylsilyl)-N-methyltrifluoroacetamid, with 1% tert-butyldimethylchlorosilane (375934 Sigma-Aldrich) for 30 minutes at 80°C. Isotopomer distributions were measured using a DB5-MS GC column in a 7890 GC system (Agilent Technologies) combined with a 5977 MS system (Agilent Technologies). Correction for natural isotope abundance and calculation of fractional contribution was performed as described elsewhere(Buescher et al., 2015).

Metabolite Quantification

Metabolites were quantified by LC-MS using HILIC Chromatography on an Acquity UPLC BEH Amide column 1.7 μm, 2.1x100 mm (polyamines) or a Luna NH2 column (all other metabolites) on a 1290 Infinity II UHPLC system (Agilent Technologies) combined with targeted detection in a 6495 MS system (Agilent Technologies). Peak areas were normalized to ^{13}C labelled internal standard (ISOtopic Solutions).

Western Blot

For western blot analysis, cells were washed with ice cold PBS and lysed in 1 x Cell Signaling lysis buffer (20 mM Tris-HCl, [pH 7.5], 150 mM NaCl, 1 mM Na_2EDTA, 1 mM EGTA, 1% Triton X-100, 2.5 mM sodium pyrophosphate, 1 mM β- glycerophosphate, 1 mM Na_3VO_4, 1 μg/mL leupeptin (Cell Signaling Technologies), supplemented with 1 mM PMSF. Samples were frozen and thawed 3 times followed by centrifugation at 20,000 x g for 10 min at 4°C. Cleared protein lysate was denatured with LDS loading buffer for 10 min at 70°C, and loaded on precast 4% to 12% bis-tris protein gels (Life Technologies). Proteins were transferred onto nitrocellulose membranes using the iBLOT 2 system (Life Technologies) following the manufacturer's protocols. Membranes were blocked with 5% w/v milk and 0.1% Tween-20 in TBS and incubated with the appropriate antibodies in 5% w/v BSA in TBS with 0.1% Tween-20 overnight at 4°C. All primary antibody incubations were followed by incubation with secondary HRP- conjugated antibody (Pierce) in 5% milk and 0.1% Tween-20 in TBS and visualized using SuperSignal West Pico or femto Chemiluminescent Substrate (Pierce) on Biomax MR film (Kodak). Optical density of the signals on film was quantified using grayscale measurements in ImageJ software (NIH) and converted to fold change. All antibodies were from Cell Signaling Technologies except for anti-ABAT, Anti-ACC, anti-Aconitase 1, anti-ASL, anti-DLD, anti-DOHH, anti-DHPS, anti-MCM, anti-ODC (Abcam), anti-eIF5A (BD Bioscience), anti-hypusine (Merck-Millipore). Electron transport chain complexes were probed with the Total OXPHOS Rodent WB Antibody Cocktail (Abcam). For T cells, we lysed cells at 40,000/μL and loaded protein from 300,000 cells per lane. For macrophages we lysed a concentration of 25,000 cell/μL and loaded protein from 175,000 cells/lane. Due to the high total eIF5A protein found in most cells, we used different parameters when blotting for this protein and its hypusinated form. To obtain a luminescent signal that produced bands in the linear range of the film with reasonable exposure times (5-30 seconds), we loaded 10-fold less protein for both T cells and macrophages, which equated to approximately 30,000 and 17,500 cells per lane, respectively.

Retroviral Transduction

In BMMφ, bone marrow cells exposed to M-CSF were transduced with luciferase (empty vector) or *Eif5a*-,*Dhps*-, or *Dohh*-expressing retrovirus by centrifugation for 90 minutes in media containing hexadimethrine bromide on day 2 of culture. Transduced cells were subsequently drug or cytokine-treated on day 7 of culture and assayed on day 8, sometimes following sorting on day 6. GFP was used as a marker for transduction in these cells.

Targeted mCherry

A G-block construct (IDT) containing mCherry fused to the degron from ODC (Kelly et al., 2007) (HGFPPEVEEQDDGTLPMSCA QESGMDRH*) (mCherry^{deg}) was constructed to reduce half-life of the mCherry fusion protein. Between the cloning sites and mCherry a Gly-Ser-Gly-Ser-Gly flexible linker was included, to allow correct and independent folding of the introduced sequences and mCherry. The mCherry^{deg} was cloned into MSCV-I-GFP using XhoI and EcoRI. MTS, NLS, or control sequences were ordered as G-blocks (IDT) or as phosphorylated oligos containg XhoI and BamHI compatible overhangs and cloned into MSCV-mCherry^{deg}-I-GFP using XhoI and BamHI. The targeted sequences fused to mCherry are denoted in Figure 3 and extended data Figure 3.

Lentiviral Transductions

The IPTG-inducible MISSION shRNA lentiviral vector pLKO-puro-IPTG-3xLacO was purchased either with a shRNA against the 3′-UTR of the murine eIF5A mRNA sequence (custom-made from #SHCLND-NM181582-TRCN0000125229; Sigma) or a corresponding non-target shRNA control (#SHC332-1EA; Sigma). Stable transduction of the lentiviral was performed as previously described(Preukschas et al., 2012) using HEK293T cells, the packaging plasmids: pMDLg/pRRE (Gag/Pol), pRSV-Rev (Rev) and phCMV-VSV-G (envelope) as well as the ProFection Mammalian Transfection System Calcium Phosphate Kit (Promega). Positive cells were selected using puromycin.

siRNA Knockdown of *Eif5a* and *Dhps* in MEFS

18 hours before transfection 750000 MEFS were plated in individual wells of a six well plate and left to attach overnight. Transfection mixes were prepared in serum free (Opti-MEM) media according to the manufacturer's recommendations. In short, 150 μL Opti-MEM per well was mixed with 3 μL DharmaFECT-3 reagent (GE Healthcare) and incubated for 5 minutes at RT. In a separate tube 150 μL of Opti-MEM was supplemented with 1 μM non targeting AF647 labeled siRNA oligo (GE Healthcare) with or without 5 μM Smartpool siRNA against *Eif5a* or *Dhps* (GE Healthcare), which consists of 4 targeting oligos each. Tubes containing reagent and siRNA mixes were mixed and incubated for 20 minutes at RT, supplemented with 1200 μl of serum free DMEM supplemented with 10% FBS (Hyclone). Medium on cells was replaced with transfection mixture and incubated for 48 hours before analysis.

Proteomics

Sample Preparation

After cell collection, protein sample preparation was carried out as described in Kulak et al. (Kulak et al., 2014) with minor modifications. In brief, macrophages were lysed in urea buffer (8 M urea, 10 mM TCEP, 40 mM CAA, and 100 mM Tris pH8.5) and protein concentration estimation was carried out using BradfordRed reagent (Expedeon). 50 μg total protein was digested with endoproteinase lys C at a ratio of 1:50 (enzyme to protein) for 3 hours at room temperature followed by dilution of the lysate to an urea concentration below 2 M and digestion with trypsin at a ratio of 1:50 (enzyme to protein) for 13 hours at 37°C. Tryptic peptides were transferred to commercial centrifugal iST devices (PreOmics) and fractionated into 3 different fractions followed by clean-up/desalting and eluted as described in (Kulak et al., 2014).

Mass Spectrometric Acquisition

General nanoLC-MS setup was similar as previously described (Engelke et al., 2014) with modifications described in the following. QExactive mass spectrometer (Thermo Fisher Scientific, Germany) and Easy nanoLC-1000 were used for all experiments. Chromatographic separation of peptides was carried out on in-house packed fused-silica emitter nanoLC columns (75 μm × 20 cm) (Silica PicoTip; New Objective, U.S.A.) packed with 1.9 μm reverse-phase ReproSil-Pur C18-AQ beads (Dr. Maisch, Germany). Peptides were separated by a 3h linear gradient of 5-80% buffer B (80% acetonitrile, 0.1% formic acid) at constant flow rate of 300 nL/min. For MS data acquisition the "fast" method from Kelstrup et al.(Kelstrup et al., 2012) was adopted.

Mass Spectrometry Data Analysis

MS raw files were analyzed by MaxQuant software and peak lists were searched against the mouse Uniprot FASTA database (concatenated with a database containing common contaminants) by the Andromeda search engine embedded in MaxQuant (Cox and Mann, 2008; Cox et al., 2011). MS1-based label free quantification (LFQ) was done using maxLFQ algorithm (Cox et al., 2014). We require a minimum of two peptide ratios in order to consider a given protein as valid (protein and peptide ID FDR=0.01). Perseus platform (Tyanova et al., 2016) was used to perform data filtering and statistical testing. In step 1, contaminant hits, reverse identification hits, and proteins "only identified by site" were removed from the dataset. In step 2, LFQ intensities were $\log_2$ transformed. This was followed by categorical annotation to create two samples groups based on their treatment. Step 3 involved removal of missing quantitative data points to minimize the number of missing values in the dataset and this was followed by missing value data imputation using a normal distribution simulating the distribution of low abundant proteins in the dataset. Lastly, Student's *t*-test was utilized to define differentially expressed proteins employing a two-fold change as a cut-off at a 5% FDR.

Flow Cytometry and Confocal Microscopy

Flow cytometric staining was performed as previously described (Chang et al., 2015). All fluorochrome-conjugated monoclonal antibodies were from (eBioscience), except for anti-CD301 (BioRad). Both NOS2 and RELMα protein levels were quantified after fixation and permeabilisation using the transcription buffer staining set (eBioscience) and monoclonal antibodies against NOS2 (Santa Cruz) and RELMα (Peprotech). eIF5A and eIF5A^{H} levels were quantified using anti-eIF5A (BD Bioscience) anti-hypusine (Merck-Millipore) after fixation and permeabilisation using the CytoFix/CytoPerm kit (BD Bioscience). Cells were stained with Live/Dead viability dye (Thermo) prior to antibody staining. Cells were collected on LSR II and Fortessa flow cytometers (BD Biosciences) and analysed using FlowJo (TreeStar) software. Cells were sorted using a FACS Aria II. Cells were imaged using a Zeiss spinning disk confocal microscope with an Evolve (EMCCD) camera. Cells were kept in a humidified incubation chamber at 37°C with 5% CO_2 during image collection. Images were deconvolved using Huygens essential software (Scientific Volume Imaging) and analysed using Imaris software (Bitplane). To verify mitochondrial localization of the MTS mCherry constructs, cell were stained with 100nM Mitotracker™ Deep Red FM (Thermo) for 30 minutes at 37°C, washed twice and analyzed using an ImageStream X Mark II Imaging Flow Cytometer (Merck Millipore).

RT-PCR

RNA was isolated using the RNeasy kit (Qiagen) and single-strand cDNA was synthesized using the High Capacity cDNA Reverse Transcription Kit (Applied Biosystems). All RT-PCR was performed with Taqman primers using an Applied Biosystems 7000 sequence detection system. The expression levels of mRNA were normalized to the expression of a housekeeping gene (β-actin).

Polysome Profile Analysis

Lysates were obtained by glass beads disruption as previously described (Jaiswal et al., 2011) in lysis buffer consisting of 20 mM HEPES-KOH pH 7.4, 100 mM KAc, 2 mM MgAc2, 2 mM DTT, 1mM PMSF, 50 μg/ml cycloheximide and protease inhibitor mix: 1.25μg/ml leupeptin, 0.75 μg/ml antipain, 0.25 μg/ml chymostatin, 0.25 μg/ml elastinal, 5 μg/ml pepstatin A. Ten absorption units (260 nm) of lysate were loaded onto linear 15%-to-55% sucrose gradients. After centrifugation at 200,000 x g for 2.5h at 4°C, gradients were separated from top to bottom into 20 fractions, from which RNA was harvested for RT-PCR.

QUANTIFICATION AND STATISTICAL ANALYSIS

Statistical analysis was performed using prism 6 software (Graph pad) and results are represented as mean ± SEM, unless otherwise indicated. Comparisons for two groups were calculated using unpaired two-tailed Student's t tests, comparisons of more than two groups were calculated using one-way ANOVA with Bonferroni's multiple comparison tests. We observed normal distribution and no difference in variance between groups in individual comparisons. Statistical significance: * $p<0.05$; ** $p < 0.005$; *** $p < 0.0005$; **** $p < 0.0001$. Further details on statistical analysis are listed in the figure legends.

DATA AND SOFTWARE AVAILABILITY

All mass spectrometry raw data are deposited to the ProteomeXchange Consortium via PRIDE repository and are accessible with the dataset identifier PXD013443.